GERMAN - MONGOLIAN INSTITUTE FOR RESOURCES AND TECHNOLOGY

The present work was submitted to the Faculty of Raw Materials and Environmental Engineering

NUMERICAL MODELING STUDY ON THE EFFECTS OF URBAN GREENING ON MICROCLIMATE

Bachelor's Thesis

by

ARIUNTSETSEG Erdenechuluun

Study program: Environmental Engineering

Student ID: B2200057

1st Supervisor/Examiner: Prof. Dr. Gantuya Ganbat

2nd Supervisor/Examiner: Prof. Dr. Jambajamts Lkhamjav

Ulaanbaatar/Nalaikh

2026

GERMAN - MONGOLIAN INSTITUTE FOR RESOURCES AND TECHNOLOGY

The present work was submitted to the Faculty of Raw Materials and Environmental Engineering

NUMERICAL MODELING STUDY ON THE EFFECTS OF URBAN GREENING ON MICROCLIMATE

Bachelor's Thesis

by

ARIUNTSETSEG Erdenechuluun

Study program: Environmental Engineering

Student ID: B2200057

1st Supervisor/Examiner: Prof. Dr. Gantuya Ganbat

2nd Supervisor/Examiner: Prof. Dr. Jambajamts Lkhamjav

Ulaanbaatar/Nalaikh

2026

Statutory Declaration

Erdenechuluun, Ariuntsetseg	B2200057
Last Name, First Name	Student ID Number

I hereby affirm in lieu of an oath that I provided the submitted bachelor thesis

NUMERICAL MODELING STUDY ON THE EFFECTS OF URBAN GREENING ON MICROCLIMATE

I did not use any sources other than those stated. In case that the work is additionally submitted on a data medium, I declare that the written and the electronic form are completely identical. The work was not submitted in the same or similar form to any examination authority.

Ulaanbaatar, Mongolia 2026.05.29	
Place, Date	Signature

Acknowledgements

I want to thank my supervisors, Prof. Dr. Gantuya Ganbat (German-Mongolian Institute for Resources and Technology) and Prof. Dr. Jambajamts Lkhamjav (National University of Mongolia), for always being there to help me, provide me expert advice, and be patient with me as I worked on this research. Their profound understanding of Ulaanbaatar's urban climate and atmospheric modeling has always inspired me.

I also want to thank Mr. B. Ganbold from the National University of Mongolia for helping me set up the high-performance computing environment that ran the WRF simulations.

The German-Mongolian Institute for Resources and Technology (GMIT) gave me the academic setting, infrastructure, and educational assistance that made this thesis feasible. Thank you very much.

Finally, I want to express my heartfelt gratitude to my family for their unwavering love, patience, and support throughout my studies. They have been my greatest source of encouragement.

Ariuntsetseg Erdenechuluun

[May 2026]

Abstract

Urban greening is widely promoted as a nature-based remedy for urban overheating, yet its microclimate response in cold, semi-arid, mountain-bounded capital cities such as Ulaanbaatar differs fundamentally from the linear cooling reported in humid climates.

The Weather Research and Forecasting model coupled to the Single-Layer Urban Canopy Model was configured in four nested domains down to 1 kilometer over Ulaanbaatar, driven by ERA5 reanalysis. Four scenarios were simulated for 22 June 2025 by modifying the urban impervious-area fraction (FRC_URB) at 1.0, 0.9, 0.5, and 0.1, corresponding to greening levels of 0, 10, 50, and 90 percent. The 0.9 case was retained as the control.

The control reproduced the tropospheric temperature profile with a root-mean-square error of 1.2°C and a nocturnal urban heat island of 2.5°C, matching the long-term observed summer mean. The daytime response was moisture-dominated: a shift from 0 to 90 percent greening lowered the 2 m air temperature by only 0.3°C but raised the surface dew point by 1.8°C. The nocturnal urban heat island declined monotonically with greening fraction and reversed sign at the strongly greened limit, falling from 3.5°C through 0.6°C at moderate greening to −2.9°C at 90 percent greening, driven by reduced heat-storage release and weakened surface roughness that allowed katabatic drainage to ventilate the basin. The −2.9°C value is an upper bound sensitive to the model soil-moisture treatment.

Intermediate rather than maximum greening minimizes the nocturnal urban heat island in a basin-confined city, and the full cooling potential is realized only when greening is combined with irrigation, permeable surfaces, and rainwater harvesting.

Keywords: *Urban Heat Island, urban greening, greening sensitivity, Ulaanbaatar, WRF model, SLUCM.*

Table of Content

1. Introduction 1
1.1. Background 1
1.2. Objectives 3
2. Literature review 3
2.1. The Urban Heat Island effect 3
2.2. Urban greening as a nature-based solution 5
2.3. WRF model and its urban scheme 6
2.4. Ulaanbaatar climate and modeling studies 7
2.5. Humidity, precipitation, and water cycle 8
2.6. Urban ventilation and air-pollution dispersion 9
2.7. Greening and air quality 10
2.8. Research gaps 11
3. Study area and methods 12
3.1. Study area 12
3.2. WRF model configuration 15
3.3. Model settings 19
3.4. Urban greening scenarios 21
3.5. UHI calculation and analysis method 22
3.6. Output variables diagnosed 24
4. Results and Discussion 24
4.1. Validation against radiosonde observations 24
4.2. Control run 26
4.3. Effect of urban greening 28
4.4. Comparison with other studies 42
4.5. Limitation of the study 45
5. Conclusion 46
5.1. Summary of key findings 46
5.2. Recommendations for sustainable urban planning and nature-based solutions 47
5.3. Future research directions 49
6. References 51
Appendix 55
Appendix A - WRF namelist.input 55
Appendix B - URBPARM.TBL modifications 58
Appendix C - Software environment 58

List of Figures

Figure 1. Conceptual contrast between the Urban Heat Island effect and the cooling effects of nature-based solutions, showing the dominant physical mechanisms in each regime. Source: UN-Habitat [12].

Figure 2. Ulaanbaatar annual climate trends from ERA5 reanalysis, 1945 to 2025.

Figure 3. Study area. (a) Topography of Mongolia. (b) Seven central districts of Ulaanbaatar with two zoom-in boxes (yellow: Ulaanbaatar urban core; red: Nalaikh). (c) Central Ulaanbaatar showing Sukhbaatar Square and the Tuul River.

Figure 4. Spatial distribution of building footprints in central Ulaanbaatar (study extent: 22 by 11 km), classified by ground-floor area.

Figure 5. Interaction between the major WRF physics parameterization modules (cumulus, microphysics, radiation, PBL, and surface) and the fluxes exchanged between them. Adapted from the WRF Users Guide [40].

Figure 6. WRF nested domain configuration: (a) D01 to D03 over East and Central Asia with D01 model terrain; (b) D04 zoom over Ulaanbaatar with high-resolution DEM.

Figure 7. Spatial framework for the UHI calculation, showing the urban grid cell at Sukhbaatar Square and the three rural reference points (Takhilt, Buyant-Ukhaa, Officer).

Figure 8. WRF CTRL (red) versus radiosonde (black) at WMO station 44292 (Ulaanbaatar) for (a) 20 LST 22 June (12 UTC, evening transition) and (b) 08 LST 23 June (00 UTC, post-inversion morning). Solid lines show temperature, dashed lines show dew-point temperature; wind barbs are from the radiosonde only.

Figure 9. (a) West to east and (b) north to south cross-sections of T2 and terrain elevation through Ulaanbaatar on 22 June 2025.

Figure 10. Three-dimensional terrain of (a) Ulaanbaatar and (b) Nalaikh in the inner domain (D04, 1 km) with 24-hour mean T2 projection. Red contour on terrain marks urban extent (FRC_URB = 0.90).

Figure 11. Surface energy balance for the Ulaanbaatar urban analysis box (106.75 to 107.05 °E, 47.87 to 47.97 °N) in the four FRC_URB sensitivity simulations.

Figure 12. Diurnal cycle of the simulated surface energy balance and boundary-layer state at the Ulaanbaatar urban center (solid lines) and the three-point rural reference mean (dashed lines) for the four FRC_URB scenarios on 22 June 2025: (a) sensible heat flux H, (b) latent heat flux LE, (c) 2 m air temperature T2, and (d) boundary-layer height.

Figure 13. Comparison of simulated vertical profiles at the Ulaanbaatar grid point in WRF D04 for the four FRC_URB sensitivity simulations on 22 June 2025: (a) daytime peak at 14 LST and (b) deep nocturnal stable layer at 05 LST. Wind barbs are shown for the CTRL run only.

Figure 14. Day versus night vertical cross-sections through the Ulaanbaatar basin in the CTRL simulation: north to south and west to east transects at 14 LST and 05 LST.

Figure 15. Vertical cross-sections through Ulaanbaatar for the four FRC_URB sensitivity simulations on 22 June 2025: (a) daytime at 14 LST 22 June and (b) night at 05 LST 23 June.

Figure 16. Urban Heat Island intensity at Ulaanbaatar (urban grid cell minus mean of three rural grid cells: Takhilt, Buyant-Ukhaa, Officer) on 22 June 2025: (a) hour-by-hour diurnal evolution for the four FRC_URB scenarios; (b) day-mean (06 to 18 LST, orange circles).

Figure 17. Three-dimensional perspective view of the simulated 24-hour mean 2 m air temperature draped over the Ulaanbaatar basin topography for the four FRC_URB scenarios: (a) NOGR (T2 max = 28.2 °C); (b) CTRL (T2 max = 28.0 °C); (c) GR50 (T2 max = 28.0 °C); (d) GR90 (T2 max = 27.9 °C). The red contour marks the urban land-use extent.

Figure 18. Plan view of 2 m air temperature (smoothly shaded) and 10 m wind vectors over Ulaanbaatar at 05 LST 23 June 2025 for the four FRC_URB sensitivity scenarios: (a) NOGR, (b) CTRL, (c) GR50, (d) GR90.

Figure 19. Near-surface temperature anomaly (ΔT2 = T2(scenario) − T2(CTRL)) at 05 LST on 23 June 2025 for three sensitivity simulations relative to CTRL: (a) NOGR, (b) GR50, and (c) GR90. Coordinates are given as distance from the Ulaanbaatar center (yellow star). Solid contours mark 0.5 and 1.0 °C; dashed contours mark −0.5 and −1.0 °C. Wind reference vector: 1 m/s.

List of Tables

Table 1. Reported UHI intensities and greening-induced cooling across representative cities.

Table 2. Counts and total ground-floor areas of building footprints in central Ulaanbaatar by class. Areas computed in UTM Zone 48N from OpenStreetMap building polygons [38].

Table 3. Physical parameterization schemes used in all WRF simulations.

Table 4. WRF nested domain configuration.

Table 5. Urban greening scenario definitions.

Table 6. Coordinates and characteristics of the urban grid point and three rural reference points used in the UHI calculation.

Table 7. Output variables diagnosed from WRF simulations.

Table 8. Summary statistics of the control-run T2 field in the two sub-domains (24-hour mean, 22 June 2025).

Table 9. Daytime (06 to 18 LST) and night-time (18 to 06 LST) means of the urban-box surface energy balance for the four FRC_URB sensitivity simulations on 22 June 2025.

Table 10. Simulated surface values (T, Td, mixing ratio QV, relative humidity RH) and differences with respect to the CTRL run at the Ulaanbaatar grid point for day and night snapshots on 22 June 2025.

Table 11. Scope and limitations of the study.

List of abbreviations

Abbreviation	Full term
AGL	Above ground level
BEP	Building Effect Parameterization
BEM	Building Energy Model
CFL	Courant–Friedrichs–Lewy stability condition
CTRL	Control simulation (FRC_URB = 0.9, Greening = 10%)
ERA5	Fifth-generation ECMWF atmospheric reanalysis
ET	Evapotranspiration
FRC_URB	Urban impervious-area fraction (SLUCM parameter)
GR50	Greening scenario 1 (FRC_URB = 0.5, 50% green)
GR90	Greening scenario 2 (FRC_URB = 0.1, 90% green)
H	Sensible heat flux (W/m²)
HFX	Sensible heat flux (WRF output variable)
HGT	Terrain elevation (m above sea level)
IGBP	International Geosphere–Biosphere Programme
LAI	Leaf area index
LE	Latent heat flux (W/m²)
LH	Latent heat flux (WRF output variable)
LCZ	Local Climate Zone classification
LSM	Land Surface Model
LST	Local Standard Time (UTC + 8 for Mongolia)
MODIS	Moderate Resolution Imaging Spectroradiometer
NDVI	Normalised Difference Vegetation Index
NOGR	No-greening reference (FRC_URB = 1.0, 0% green)
Noah LSM	Noah Land Surface Model
PBL	Planetary Boundary Layer
PBLH	Planetary boundary-layer height (m)
RH	Relative humidity (%)
RMSE	Root-Mean-Square Error
RRTMG	Rapid Radiative Transfer Model for global applications
SLUCM	Single-Layer Urban Canopy Model
TSK	Surface skin temperature (K)
T2 / T2	2-m air temperature
Td	Dew-point temperature (°C)
UB	Ulaanbaatar
UCM	Urban Canopy Model
UHI	Urban Heat Island
URBPARM.TBL	WRF urban parameter lookup table
UTC	Coordinated Universal Time
UTM	Universal Transverse Mercator (projection)
WMO	World Meteorological Organization
WPS	WRF Preprocessing System
WRF	Weather Research and Forecasting model
WSM6	WRF Single-Moment 6-Class microphysics scheme
YSU	Yonsei University planetary boundary-layer scheme
β	Bowen ratio (= H / LE)
α	Surface albedo
ε	Surface emissivity
θ	Volumetric soil moisture (m³/m³)
ΔT, ΔTd	Temperature / dew-point difference between scenarios (°C)
Δx	Horizontal grid spacing

1. Introduction

1.1. Background

Accelerating urbanization is one of the defining environmental challenges of the twenty-first century. More than half of the world's population currently lives in cities, and projections show this share will approach 70% by 2050 [1]. Urban expansion systematically transforms natural land surfaces, grassland, forest, and bare soil into impervious materials such as asphalt, concrete, and roofing, fundamentally altering the partitioning of energy at the land–atmosphere interface. The replacement of vegetated surfaces reduces ET, increases solar-radiation storage in urban fabrics, and traps outgoing longwave radiation within street canyons [2]. The cumulative result is the Urban Heat Island (UHI) effect: a persistent elevation of near-surface air temperature in cities relative to their surrounding rural environments, with annual-mean magnitudes of 1-3°C in mid-latitude cities and peaks exceeding 5°C during heat waves [2], [3].

The drivers of UHI formation are well established: low albedo and high thermal mass of impervious surfaces, reduced sky-view factors in dense canyons, and anthropogenic heat from transport, buildings, and industry [3]. Urban greening, the deliberate expansion of vegetation through parks, street trees, green roofs, and corridors, has emerged as one of the most effective nature-based mitigation strategies. Vegetation cools cities through shading and ET (evapotranspiration), converting sensible heat into latent heat through transpiration and bare-soil evaporation [1]. A meta-analysis by Bowler et al. [4] of 71 studies reported a mean cooling magnitude of 0.9°C for parks, with the largest cooling under sunny, low-wind conditions over well-watered vegetation. A decade-long systematic review confirmed consistent air-temperature reductions of 1–5°C from urban green space, with cooling strongly moderated by water availability in arid and semi-arid settings [1].

The local climate response is governed primarily by the urban-fraction parameter FRC_URB. As FRC_URB decreases, the surface energy balance shifts in three coupled ways: (i) surface albedo rises modestly as vegetation reflects more shortwave radiation than aged asphalt, reducing absorbed net radiation; (ii) latent heat flux (LE) rises sharply through transpiration while sensible heat flux (H) falls by a comparable magnitude, directly cooling the near-surface air; and (iii) the thermal mass of the urban canopy decreases, reducing the daytime-stored heat that is released as nocturnal longwave radiation [3], [5]. Together these mechanisms imply a decrease in mean and peak air temperature with increasing vegetation fraction, with the largest cooling typically

observed in dry, sunny, low-wind daytime conditions precisely the meteorological setting of Ulaanbaatar in summer.

Table 1. Reported UHI intensities and greening-induced cooling across representative cities.

Metric	Range	Source
Typical UHI intensity (annual mean, mid latitude cities)	1-3°C	[3]
UHI intensity during heatwaves	up to 5+ °C	[3]
Mean cooling from urban green space (meta-analysis)	0.94°C	[4]
Cooling from urban green space (humid climates)	1-5°C	[1], [4]
Cooling from urban green space (semi-arid climates)	1-5°C, water-limited	[1], [5]
Observed summer daily max UHI, Ulaanbaatar	2.5°C	[5]
Observed winter mean UHI, Ulaanbaatar:	3.3°C	[5]

Ulaanbaatar, the capital of Mongolia, presents a particularly compelling case for UHI research. The city sits at approximately 1350 m elevation in a narrow valley bounded by mountain ranges, Bogd Khan Uul to the south and branches of the Khentii range to the north. Observations from 31 years of station data (1980-2010) documented a mean annual UHI of 1.6°C, a summer mean of 0.3°C with summer daily maxima averaging 2.5°C, and a winter mean of 3.3°C with winter daily maxima averaging 6.4°C [5]. Ulaanbaatar's UHI is superimposed on a strong regional warming signal: Mongolia's near-surface temperature has risen by approximately 2.4°C between 1940 and 2022, with winter warming of 3.2°C and summer warming of 1.6°C [7]. The city's population grew from 0.8 million in 1999 to 1.7 million by 2024 [8], and its built-up area has nearly doubled since 1974 [5], [6]. This combination of rapid urbanization, topographic confinement, extreme continental warming, and very limited background vegetation makes Ulaanbaatar one of the most thermally stressed capital cities in the world.

Numerical modeling provides the only controlled framework for disentangling individual contributions of land-surface modifications to urban microclimate. The WRF model coupled with the Noah LSM and a suite of UCMs has become the most widely used mesoscale tool for this purpose [9], [10]. The WRF/urban system splits each grid cell into an impervious urban fraction (FRC_URB) and a vegetated fraction handled by Noah LSM; reducing FRC_URB directly increases evapotranspiration (ET) and decreases H in proportion to the added green area [9]. Previous WRF studies for Ulaanbaatar have focused on urban breeze circulations and valley-mountain interactions [6], [11], but no published work has applied systematic greening scenario experiments to the city's land surface. The present study addresses this gap using the WRF/SLUCM framework to evaluate microclimate responses across a comprehensive range of urban vegetation fractions.

This thesis asks: how sensitive is Ulaanbaatar's summer microclimate to the urban vegetation fraction, and does the response in this cold, semi-arid, mountain-bounded basin follow the linear cooling pattern reported for other climates?

1.2. Objectives

This study pursues five interconnected objectives, aligned with the goals of the thesis assignment:

1. Review existing research on urban heat island (UHI) mechanisms, urban greening effects, WRF-based urban modeling, and Ulaanbaatar's climatic and land-surface characteristics, and use this review to design a physically motivated set of greening scenario experiments.
2. Simulate the effects of varying urban vegetation fractions on the surface energy balance by modifying FRC_URB in the WRF/SLUCM framework and comparing scenarios against a control run representing current Ulaanbaatar land-use conditions.
3. Analyze changes in net radiation, H, LE, and ground heat flux across the full set of greening and de-greening scenarios to identify the physical mechanisms driving temperature changes.
4. Evaluate the sensitivity of 2m air temperature (T2) and skin temperature (TSK) to the degree of urban greening, testing vegetation fractions corresponding to 0% (NOGR, FRC_URB=1.0), 10% (CTRL, FRC_URB=0.9), 50% (GR50, FRC_URB=0.5), and 90% (GR90, FRC_URB=0.1) green coverage.
5. Translate the simulated findings into actionable recommendations for sustainable urban planning in Ulaanbaatar, identifying the spatial and operational design principles under which urban greening interventions are likely to deliver the largest microclimate benefit.

2. Literature review

2.1. The Urban Heat Island effect

The UHI is among the most extensively documented phenomena in urban climatology. Oke [2] established the energetic basis of the effect: the replacement of natural vegetated surfaces with impervious materials fundamentally alters the surface energy balance by reducing the Bowen ratio partitioning of available energy between latent and sensible heat and by trapping longwave radiation within street canyons. The outcome is systematically elevated surface and near-surface air temperatures within city boundaries relative to surrounding rural areas.

The drivers of UHI formation can be grouped into three categories. First, the physical properties of impervious surfaces, low albedo, high thermal mass, and low moisture availability promote daytime heat storage and nocturnal release. Second, urban canyon geometry reduces the sky-view factor and traps outgoing longwave radiation, amplifying the nocturnal component of the UHI. Third, anthropogenic heat from transport, buildings, and industry provides a direct thermal load, particularly important in cold seasons and

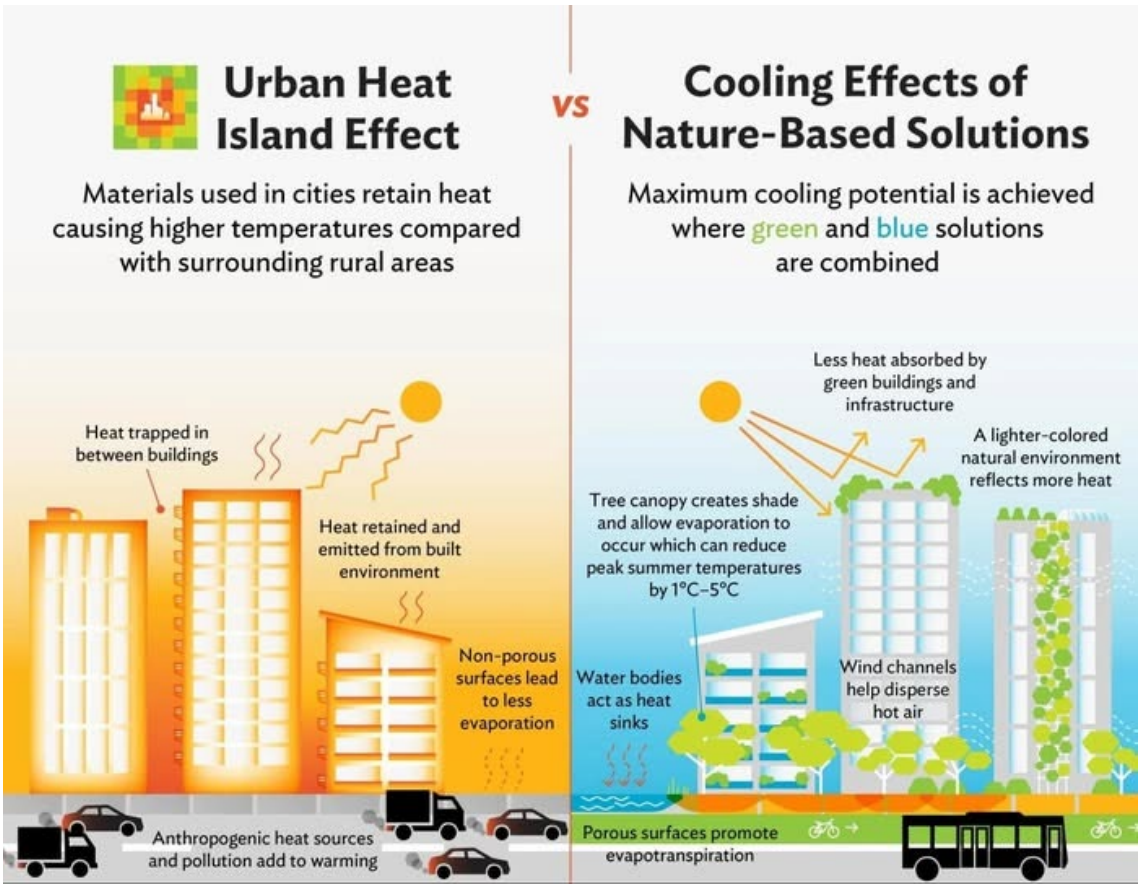


Figure 1. Conceptual contrast between the Urban Heat Island effect (left) and the cooling effects of nature-based solutions (right), showing the dominant physical mechanisms in each regime. Source: UN-Habitat [12]

high-density districts. Typical UHI intensities range from 1°C to 3°C but can reach 5-8°C during heatwaves, and long-term observational studies report continuing intensification in line with urban expansion.

Figure 1 contrasts the two regimes that the present study investigates side by side. The left panel illustrates the conventional UHI mechanism: in densely built urban fabric, low-albedo materials store daytime shortwave radiation, deep street canyons trap outgoing longwave radiation between buildings, non-porous surfaces suppress evaporation, and anthropogenic heat from transport and buildings adds a direct thermal load, all of which combine to elevate near-surface air temperature relative to the surrounding rural

environment. The right panel summarizes the nature-based solutions that this thesis evaluates through the FRC_URB sensitivity experiment: tree canopies provide shade and convert absorbed shortwave radiation into latent heat through evapotranspiration, lighter and more vegetated surfaces reflect a larger share of incoming radiation, water bodies act as local heat sinks, and porous vegetated surfaces sustain soil moisture available for evapotranspiration. Reported air-temperature reductions of 1-5°C from these combined mechanisms [12] are consistent with the meta-analytic mean of 0.9°C reported by Bowler et al. [4] and bound the range of cooling magnitudes that the FRC_URB scenarios in Chapter 4 are designed to reproduce for the specific case of Ulaanbaatar.

2.2. Urban greening as a nature-based solution

Urban greening cools cities through two mechanisms that operate simultaneously but are not equally effective in every climate, and recognising this distinction is essential for interpreting the results that follow. Shading interrupts the direct shortwave load on impervious surfaces, while evapotranspiration redirects absorbed energy from the sensible to the latent pathway, cooling both the radiating surface and the air immediately above it [13]. The two mechanisms differ fundamentally in their water dependence: shading operates as long as canopy cover is present, whereas evapotranspiration is bounded by the soil-moisture reservoir feeding the vegetation. This asymmetry sets up a climate-dependent hierarchy of cooling potential.

The empirical record bears this out. Bowler et al.'s [4] meta-analysis of 71 case studies found a mean park-cooling magnitude of 0.9°C, but the spread around this mean is the more informative quantity: cooling reached almost 3°C under tree canopies during the day and collapsed to roughly 0.5°C at night, indicating that the daytime shading-plus-ET component is far stronger than the nocturnal radiative-only component. Soltanifard and Amani-Beni's [1] decade-long systematic review extended this conclusion across climate zones and identified water availability as the single most decisive moderator of cooling magnitude in arid and semi-arid settings precisely the regime to which Ulaanbaatar belongs. The Melbourne 2009 heatwave produced cooling of up to 3°C [14] in a temperate, irrigated context, while Mohammed et al.[15] showed that desert urban environments respond primarily through TSK reduction rather than T2 reduction. These results are not interchangeable case studies; they are evidence that the same greening intervention produces qualitatively different microclimate signals depending on the moisture environment.

This climate dependence has direct implications for how the WRF/SLUCM framework should be applied to Ulaanbaatar. Within SLUCM, FRC_URB is the only mechanism through which vegetation fraction enters the surface energy balance: lowering FRC_URB increases the fraction of each grid cell handled by Noah LSM, which in turn raises ET in proportion to the available soil moisture. In humid climates this yields a near-linear cooling response, but in semi-arid climates the soil-moisture ceiling caps the realized latent flux long before the available radiative energy is converted, and the dominant outcome shifts from temperature reduction to atmospheric humidification. The present study is the first to apply this framework to Ulaanbaatar or any Mongolian city; the results in Sections 4.3.3 and 4.3.4 confirm that the moisture-dominated daytime regime predicted on theoretical grounds does in fact emerge in the simulations.

Local empirical evidence reinforces the case for an Ulaanbaatar-specific WRF investigation rather than reliance on transferred conclusions from other climates. An i-Tree Eco analysis of the Songinokhairkhan ger district [16], based on a 2025 inventory of 6,446 urban trees and 2017 air quality observations, established a near-linear relationship between green-cover fraction and annual pollutant removal: each additional 10% of green cover delivers approximately 102-105 kg/yr of removal capacity, valued at MNT 66.4 million per year. The pollutant-removal pathway operates year-round and is mechanistically distinct from the microclimate cooling investigated here, but it confirms that urban greening in Ulaanbaatar delivers measurable, scalable environmental benefits which is the prerequisite for treating the FRC_URB sensitivity experiment as a policy-relevant question rather than a purely academic exercise.

2.3. WRF model and its urban scheme

The integrated WRF/urban modeling system [9] combines the non-hydrostatic atmospheric dynamical core of WRF [10] with the Noah LSM and a collection of UCMs. There are three UCMs: SLUCM [17], the multi-layer building effect parameterization (BEP), and the combination BEP+BEM. Single layer urban canopy model (SLUCM) models the urban surface as an endlessly long, uniform two-dimensional street canyon with three geometric parameters: building height (ZR), building width (BW), and road width (SW). It also takes into account the thermophysical qualities of roofs, walls, and roadways. The plan clearly defines how shortwave and longwave radiation can be blocked, reflected, and trapped in the canyon; how heat can be stored in the materials used for the roof, walls, and roads; and how fast the canyon and the air above it can move and how turbulent the transfer coefficients can be.

For cities with average building heights and not too many tall buildings, like Ulaanbaatar, SLUCM strikes a good compromise between physical realism and computing expense. Numerous studies have utilized FRC_URB-based scenario trials within SLUCM to measure the microclimate's response to variations in vegetation fraction [14], [15], [18] which is the exact strategy employed in this case. The multi-layer BEP and BEP+BEM systems are better for big cities with plenty of tall buildings, but they aren't needed for Ulaanbaatar's urban morphology.

The community WRF physics suite couples SLUCM to several established schemes for atmospheric processes [10]: the WSM6 microphysics scheme [19]; the Kain–Fritsch cumulus scheme [20] (active only in the outermost domains); RRTMG for both shortwave and longwave radiation [21]; the YSU planetary boundary-layer scheme [22]; and the Noah LSM [23]. Each of these is described in detail in Section 3.2.2.

2.4. Ulaanbaatar climate and modeling studies

Ulaanbaatar occupies a topographic and climatic configuration that is unusual among capital cities and that, taken together, makes the city a particularly diagnostic test case for urban-greening modeling. The city sits at approximately 1350m elevation in a broad east–west valley along the Tuul River, bounded by Bogd Khan Uul to the south (peak 2260m) and branches of the Khentii range to the north (peak 2800m). Its cold semi-arid continental climate (Köppen BSk) combines limited background vegetation, intense summer solar radiation, and extremely cold dry winters. Each of these features is found individually in other urban-climate studies; the combination semi-arid moisture limitation plus basin confinement plus high elevation plus sparse natural vegetation is not, and it is precisely this combination that the literature has identified as the least-studied regime in global urban-climate research [1], [24].

The case for treating Ulaanbaatar as a distinct regime rather than a variant of better-studied semi-arid cities rests on the regional climate trajectory. National-scale warming reached approximately 2.1°C between 1940 and 2009 [7], and the present study’s ERA5-based analysis (Fig. 1) extends this record through 2025 and confirms a continued warming trend of 0.2°C per decade for the Ulaanbaatar study area roughly twice the global mean rate. Mongolia's mean annual temperature rose by 0.9°C between 2000 and 2024, with the most rapid warming concentrated in March (>1°C per decade) [7]. These trends are consistent with observations from neighbouring Inner Mongolia, where Hu et al. [25] reported warming of 0.4-0.5°C per decade together with progressive drying. Two implications follow. First, the UHI signal in Ulaanbaatar is superimposed on a regional warming background that is itself accelerating, so the policy question is not whether to

mitigate but how. Second, vegetation dynamics are co-evolving: maximum NDVI across Mongolia has increased by 0.025 units per decade and gross primary productivity has risen by 38% since 2000 [26], meaning that the soil-moisture and ET environment in which any greening intervention would operate is itself non-stationary.

Against this background, the existing WRF literature on Ulaanbaatar is informative but incomplete.Ganbat & Baik [6] documented the structure of urban breeze circulations driven by the UHI, showing that convergent inflow from the surroundings into the heated urban core organizes a thermally driven circulation cell that influences pollutant dispersion and near-surface winds. Ganbat et al. [11] extended this analysis to the interaction between urban breezes and mountain slope winds, demonstrating that under calm clear-sky summer conditions the superposition produces complex diurnally-varying patterns and an elevated nocturnal temperature inversion that traps cold air at the valley floor. These studies establish two facts that the present work depends on: WRF/SLUCM reproduces the dominant dynamical features of Ulaanbaatar's urban boundary layer, and the basin's nocturnal stratification is sufficiently strong to make any greening response sensitive to roughness-mediated drainage processes. Neither study, however, modified the land surface itself; both treated the urban fabric as a fixed boundary condition and varied only the dynamical or thermal forcing. The land-surface sensitivity question that this thesis addresses what happens when FRC_URB is changed has therefore not been asked for Ulaanbaatar before, and the dynamical machinery validated by Ganbat & Baik [6] and Ganbat et al. [11] is exactly the machinery that produces the U-shaped nocturnal response identified in Section 4.3.2.

2.5. Humidity, precipitation, and water cycle

The microclimate response to urban greening is not limited to near-surface temperature. Vegetation modifies the surface water budget through three coupled mechanisms interception, infiltration, and evapotranspiration each of which feeds back into the boundary-layer atmosphere on a different timescale and is captured to a different degree by the WRF/SLUCM framework adopted in this thesis.

The most immediate effect is on near-surface humidity. Yang et al..[27] used mobile measurements across 15 cities along a climate-wetness gradient and reported that the daytime air-temperature reduction inside green spaces is largely offset by a corresponding humidity increase, leaving the wet-bulb temperature change statistically insignificant during the day; a net reduction in humid heat of approximately 0.35°C only emerges at night, and only in climates wetter than approximately 180 mm of summer precipitation. This finding is directly relevant to Ulaanbaatar's regime, where summer

precipitation is around 20-270 mm but distributed across short convective events with low antecedent soil moisture, and supports the moisture-dominated daytime response simulated in Section 4.3.3 (ΔTd up to 1.8°C against ΔT2 of only −0.3°C).

At regional scale, urban greening can modify precipitation itself. Lal et al. [28] showed using high-resolution WRF simulations over India that a stepwise increase in leaf area index intensifies terrestrial evapotranspiration and promotes downwind precipitation, with the magnitude of the effect proportional to the greening intensity. Conversely, Liang et al. [15] documented for the Greater Bay Area of South China that urban land cover suppresses winter precipitation in synoptic regimes where cold-air intrusion overwhelms the urban heat island, but enhances it where the UHI persists and amplifies local moisture-flux convergence. Both directions of the response are relevant to Ulaanbaatar: the strong summer UHI documented by Ganbat et al. [5] and reproduced by the present CTRL run (Section 4.3.6) provides a thermodynamic environment in which moderate greening could plausibly enhance, rather than suppress, summer convective precipitation, although verifying this would require an ensemble of simulations across multiple synoptic types and is beyond the scope of the present single-day experiment.

Finally, vegetation alters the urban hydrological cycle on the surface. Zheng et al. [29], in a global synthesis of 75 peer-reviewed green-roof studies, reported a mean stormwater retention rate of 62% with substantial variability driven by rainfall intensity, substrate depth, and vegetation type. The Noah land-surface model coupled to WRF/SLUCM in the present configuration solves the four-layer soil-water budget through the Richards equation (Section 3.2.3, eq. 8) but does not represent infiltration through engineered green-roof or pervious-pavement substrates explicitly; this limitation is acknowledged in Section 5.3 and motivates the recommendation that future Ulaanbaatar greening studies adopt the updated WRF v4.3+ urban scheme of Salamanca et al. [30], which introduces explicit green-roof, irrigation, and impervious-surface evaporation parameterizations.

2.6. Urban ventilation and air-pollution dispersion

The microclimate cooling potential of urban greening is intimately coupled to the city's ventilation regime, and this coupling is particularly consequential for Ulaanbaatar because the basin's poor ventilation is the primary physical driver of the wintertime air-pollution crisis [31]. Analysing 1991-2020 meteorological observations and radiosonde profiles, classified Ulaanbaatar's wintertime air-pollution potential as "very high" (ventilation coefficient below 4,000 m²/s), driven by a near-surface temperature inversion that suppresses turbulent mixing and by mountain-driven convergent flow that channels

polluted air toward the city center. Ganbat and Baik [32] used WRF coupled with the Seoul National University Urban Canopy Model (SNUUCM) to confirm numerically that the inversion layer is deeper and stronger inside the valley than over the surrounding mountain slopes, weakens during daytime as solar heating strengthens, and produces upslope and up-valley flow during the day but down-slope and down-valley flow at night.

Beyond Ulaanbaatar, a substantial body of literature has investigated whether intentionally designed urban ventilation corridors (UVCs) linear strips of low-roughness land, often vegetated can mitigate both UHI and air pollution. Liu et al. [34] simulated the introduction of UVCs in Beijing using WRF/UCM and reported a reduction in mean urban temperature of 0.18°C, an increase in wind speed of 0.33 m/s, and an increase in relative humidity of 2.83%, with corresponding improvements in pollutant dispersion. Integrated remote-sensed land-surface temperature and PM2.5 fields with WRF/BEP simulations to design optimized UVCs for Shanghai, demonstrating that corridor placement aligned with the prevailing wind direction is more effective than corridor density alone. Xu et al. [33], however, cautioned that pollutants emitted from street canyons adjacent to UVCs can migrate into the corridor itself and degrade its air-cleansing function, especially under low-wind conditions a finding directly relevant to Ulaanbaatar's wintertime stagnation regime.

The implications for the present study are twofold. First, the U-shaped nocturnal UHI response identified in Section 4.3.4 is mechanistically tied to roughness-mediated katabatic ventilation: the strongly-greened scenario (GR90) reduces aerodynamic roughness and accelerates basin-floor cooling, which acts as a natural ventilation pathway analogous to an engineered UVC. Second, the spatial pattern recommended in Section 5.2 tree-lined corridors aligned with the principal drainage axes from the Khentii Nuruu and Bogd Khan slopes, rather than uniform basin-wide greening is consistent with the design principles validated by [34], and would simultaneously enhance summertime nocturnal cooling and wintertime pollutant dispersion if combined with appropriate setback distances from major emission sources [33].

2.7. Greening and air quality

A common assumption in popular and policy discourse is that increased urban greening directly improves air quality through dry deposition on leaf surfaces. The most rigorous global synthesis to date, by Venter et al. [33], analyzed 2,615 air-quality monitoring stations across Europe and the United States and found that a one-standard-deviation increase in total green-space cover was associated with a statistically insignificant 0.8±2.7% reduction in pollutant concentrations averaged across pollutants. The effect of

trees specifically was somewhat larger but still modest (1.4±2.5% reduction averaged across pollutants, 2.7% for particulate matter) and was an order of magnitude smaller than the effect of meteorological drivers' humidity, wind speed, and precipitation on pollutant deposition and dispersion. At street scale (15-60 m radius), green space was found to restrict ventilation and slightly worsen local pollutant concentrations, an effect that becomes negative only when integrated to neighbourhood and city scales (12-16,000 m radius).

This evidence reframes the role of urban greening for air quality in Ulaanbaatar. The local i-Tree Eco analysis of the Songinokhairkhan ger district [16] established that the city's existing tree inventory removes approximately 102-105 kg of pollutants per year per 10% of green cover, equivalent to MNT 66.4 million in annual ecosystem-service value. This is a real and quantifiable benefit. However, the same global meta-analysis [33] indicates that the dominant air-quality benefit of increased greening will not arise from leaf-surface deposition but from the meteorological pathway: increased near-surface humidity, modified wind speed, and modified atmospheric stability exactly the variables that the present WRF/SLUCM experiment quantifies in Section 4.3. Specifically, the 1.8°C increase in surface dew-point and the 0.55 g/kg increase in mixing ratio simulated under GR90 (Table 10) act on pollutant deposition through wet scavenging, and the modified katabatic ventilation documented in Section 4.3.5 acts on pollutant dispersion through enhanced mechanical mixing. The implication is that air-quality benefits should be evaluated jointly with microclimate benefits in any integrated greening assessment for Ulaanbaatar, and not as an independent additive co-benefit.

2.8. Research gaps

To the best of the author's knowledge, no published study has applied WRF-based urban greening scenario experiments to Ulaanbaatar or to any Mongolian city. Existing WRF studies for Ulaanbaatar have focused on dynamical circulations rather than land-surface sensitivity. Moreover, the physical mechanisms of vegetation-induced cooling in a cold, semi-arid, high-elevation city with extremely sparse background vegetation differ substantially from those in humid or temperate climates, where most prior greening studies have been conducted. Recent global syntheses [1, 21] have identified the semi-arid, water-limited regime as one of the least-studied and most physically distinctive urban-climate categories. Finally, published FRC_URB sensitivity studies rarely span the full physically plausible range from fully impervious to near-fully vegetated. The present study addresses all three gaps by applying a four-scenario FRC_URB sensitivity experiment specifically for Ulaanbaatar, spanning FRC_URB values of 0.1 (GR90), 0.5 (GR50), 0.90 (CTRL), and 1 (NOGR).

3. Study area and methods

3.1. Study area

3.1.1. Geographic setting

Mongolia's capital and largest city, Ulaanbaatar (47.92°N, 106.85°E), is located in a vast valley along the Tuul River at around 1350m above sea level. Southern mountain ranges, especially Bogd Khan Uul, limit air drainage and local circulation [5]. The vegetation cover is restricted to steppe grassland and sparse flora, with a high concentration of trees in parks. The mean population density of Ulaanbaatar is 382.1 persons/km^2, with approximately 1,677,645 inhabitants residing in nine administrative districts, which is nearly half of the national population, and is spread across 4,704 km^2 [8]. Inventoried urban vegetation in the city's built settlement zone totals approximately 1,204,737 trees and shrubs of 75 species growing on 4.27 km² of designated green space, equivalent to about 256 plants/km² across the 4,704 km² administrative territory [35].

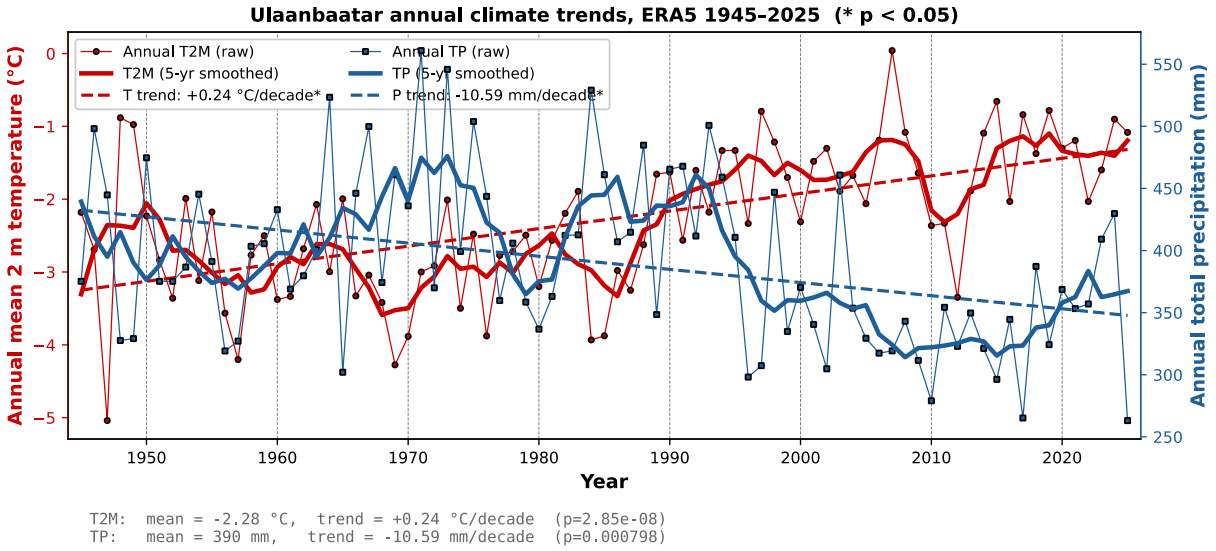


Figure 2. Ulaanbaatar annual climate trends from ERA5 reanalysis [26], 1945-2025.

Figure 2 shows the parameters that drives Ulaanbaatar urban climate. Since 1945, annual mean temperature has climbed by 0.2°C per decade ($p<0.001$), double the global average, while precipitation has declined by –10.6 mm per decade ($p<0.001$) by using ERA5 reanalysis data [36]. This warming-and-drying combination, enhanced locally by the UHI effect (1-5°C of extra warmth over built-up surfaces [3]), causes vegetation and residents to experience increased thermal stress. In such climates, increasing urban green cover is one of the best nature-based mitigation measures [37]. Figure 3 shows the location of the study area within Mongolia.

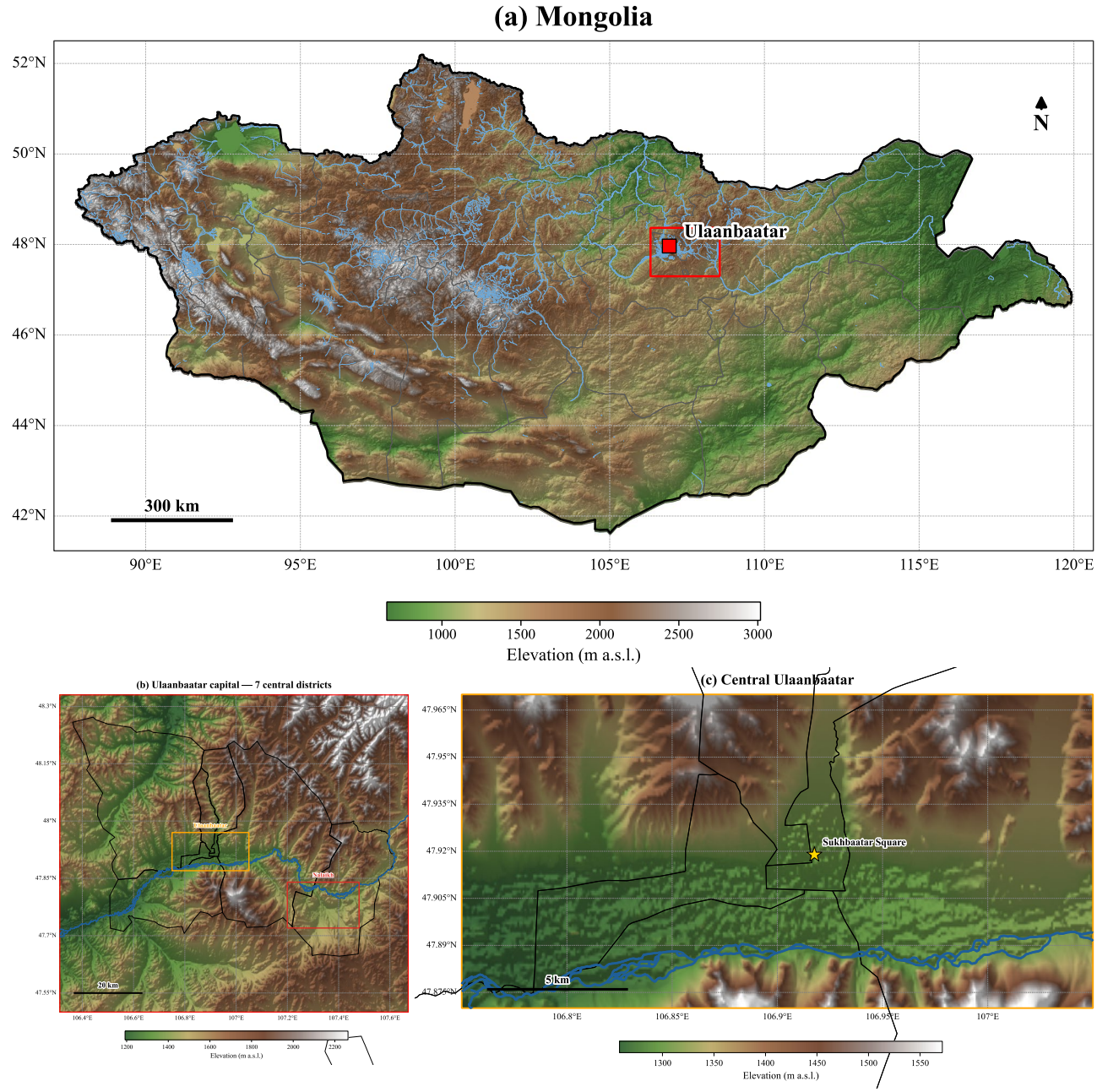


Figure 3 . Study area. (a) Topography of Mongolia. (b) Seven central districts of Ulaanbaatar with two zoom-in boxes (yellow: Ulaanbaatar urban core; red: Nalaikh). (c) Central Ulaanbaatar showing Sukhbaatar Square and the Tuul River [18].

3.1.2. Urban morphology

Figure 4 maps the footprints of all 171,402 OpenStreetMap [38] registered buildings in the study extent, classified into three groups by ground-floor area: low-density (<80 m^2), high-density (80-300 m^2), and commercial/large (>300 m^2). Table 2 summarizes counts and total covered areas for each class.

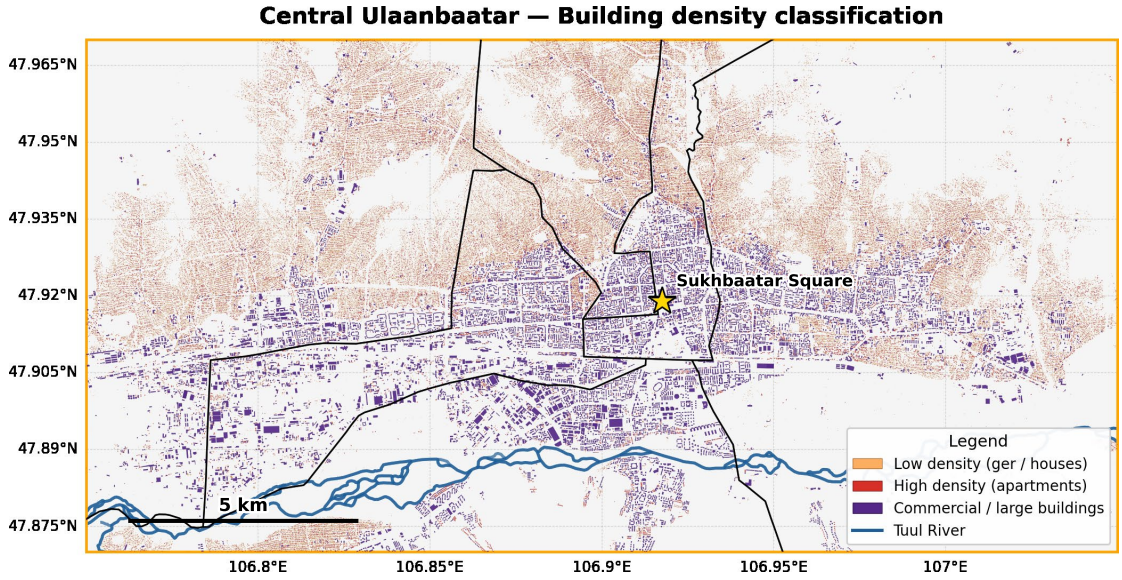


Figure 4 Spatial distribution of building footprints in central Ulaanbaatar (study extent: 22 × 11 km), classified by ground-floor area.

There is a significant difference between the city's main metropolitan core and the ger districts that surround it. Most of the buildings (71.7%) are low-density, which means they are modest structures like ger-district homes and detached single-family homes that are grouped together on hillslopes and on the edges of the city. Mid-rise apartment buildings (80-300 m^2) make up 21.2% of the total, whereas major commercial and institutional buildings (>300 m^2) make up only 7.2%. But when you look at the overall area of the ground floor, the picture changes: the 12,266 large buildings encompass 11.41 km^2, which is more than half (54.8%) of the total developed footprint of 20.80 km^2.

Table 2. Counts and total ground-floor areas of building footprints in central Ulaanbaatar by class. Areas computed in UTM Zone 48N from OpenStreetMap building polygons [38].

Building class	Count	Count, %	Total area, km²	Area, %
Low density (< 80 m^2)	122,832	71.7	4.73	22.7
High density (80–300 m^2)	36,304	21.2	4.66	22.4
Commercial / large (>300 m^2)	12,266	7.2	11.41	54.8
Total	171,402	100.0	20.80	100.0

3.2. WRF model configuration

3.2.1. Mathematical foundation: WRF dynamical core

The WRF model solves a fully compressible, non-hydrostatic version of the Navier-Stokes equations on an Eulerian mass-coordinate grid [10]. The momentum equations describing the atmospheric flow are written in flux form for the prognostic variables (μu, μv, μw), where $\mu = p_s - p_t$ is the column mass and (u, v, w) are the velocity components. In compact vector notation, the system reduces to:

$$\frac{\partial U}{\partial t} + (\nabla \cdot Vu) - \left(\frac{\partial (p\alpha)}{\partial x}\right)\left(\frac{\partial \eta}{\partial x}\right) + \left(\frac{\partial p}{\partial \eta}\right)\left(\frac{\partial \eta}{\partial x}\right) = F_U + D_U \quad (1)$$

where U = μu, V is the contravariant velocity vector, α is the inverse density, p is hydrostatic pressure, η is the terrain-following vertical coordinate, F_U represents physical forcings (Coriolis, curvature, friction, and parameterised physics), and D_U represents numerical diffusion. The full system additionally includes prognostic equations for μ (mass conservation), Θ (potential temperature), φ (geopotential), and water-substance variables.

The Navier-Stokes equations in their general form represent one of the seven Millennium Prize Problems identified by the Clay Mathematics Institute [39], for which the existence and smoothness of solutions in three dimensions remain open mathematical questions. WRF therefore solves the equations numerically using a third-order Runge-Kutta time-integration scheme combined with finite-difference (horizontal) and finite-volume (vertical) discretisations on a staggered Arakawa-C grid [10]. The numerical solution is conditionally stable under the CFL condition, which determines the time-step values reported in Table 3.

3.2.2. Physical parameterization schemes

WRF represents atmospheric processes through a set of interacting physics parameterization schemes. Figure 5 shows that WRF surface physics consists of surface-layer (sfclay) schemes and LSMs. Surface-layer schemes determine surface-layer diagnostics, including exchange and transfer coefficients, and provide these to the LSM, which in turn provides land-surface fluxes to the PBL [40]. The CONUS physics

suite was adopted as the baseline configuration with minor modifications appropriate to Mongolia's cold semi-arid conditions. Table 4 summarizes the selected schemes.

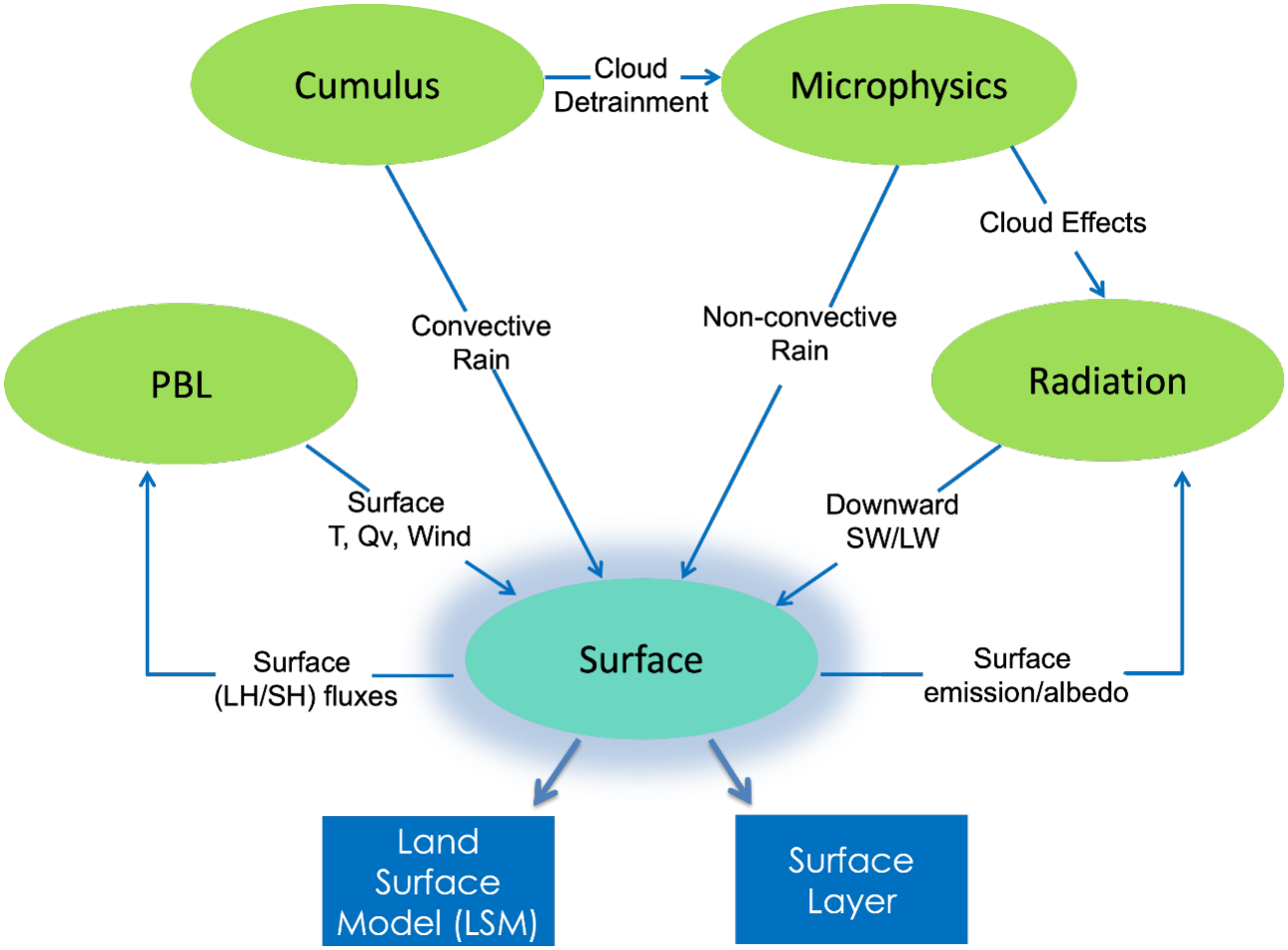


Figure 5 Interaction between the major WRF physics parameterization modules: cumulus, microphysics, radiation, PBL, and surface and the fluxes exchanged between them. Adapted from the WRF Users Guide [40]

Table 3. Physical parameterization schemes used in all WRF simulations.

Process	Scheme	Code	Reference
Microphysics	WSM6 - WRF Single-Moment 6-class	mp_physics = 6	Hong & Lim (2006) [19]
Shortwave radiation	RRTMG	ra_sw_physics = 4	Iacono et al. (2008) [21]
Longwave radiation	RRTMG	ra_lw_physics = 4	
Surface layer	Revised MM5 Monin–Obukhov	sf_sfclay_physics = 1	Skamarock et al. [10]
Land surface	Noah LSM	sf_surface_physics = 2	Tewari et al. (2004) [23]
PBL	YSU	bl_pbl_physics = 1	Hong et al. (2006) [22]
Cumulus	Kain–Fritsch (D01, D02); off (D03, D04)	cu_physics = 1 / 0	Kain (2004) [20]
Urban canopy	SLUCM	sf_urban_physics = 1	Kusaka et al. (2001) [17]

Cumulus parameterization was turned off in D03 and D04, where convection is clearly shown. We picked RRTMG because it can measure radiative transfer at different wavelengths, which is useful for comparing the radiative balance of the surface in different greening scenarios. YSU was chosen since it has been shown to work well on semi-arid land. The Noah LSM solves the four-layer soil-water and soil-temperature budget [23] using hydraulic functions based on the Clapp-Hornberger formulation. It also solves the Richards equation for soil-moisture redistribution internally at every time step over the vegetated fraction (1−FRC_URB) of each grid cell.

3.2.3. Surface energy balance equation

The thermodynamic response of the surface and the near-surface atmosphere to changes in FRC_URB analyzed in Chapter 4 emerges from the surface energy-balance closures applied within WRF over the impervious and vegetated fractions of each grid cell. The seven principal equations governing these closures are summarized below.

(1) Surface energy balance:

$$R_n = H + LE + G \quad (2)$$

(2) Net radiation:

$$R_n = (1 - \alpha)S\downarrow + \varepsilon L\downarrow - \varepsilon \sigma T_s^4 \quad (3)$$

(3) Sensible heat flux:

$$H = \rho c_p C_h |U| (T_s - T_a) \quad (4)$$

(4) Latent heat flux:

$$LE = \rho L_v C_q |U| (q_s - q_a) \quad (5)$$

(5) Stomatal resistance (Jarvis-type, Noah LSM [23]):

$$r_s = \frac{r_s,min}{LAI \cdot F1(S\downarrow) \cdot F2(VPD) \cdot F3(T_a) \cdot F4(\theta)} \quad (6)$$

(6) Ground heat flux:

$$G = \kappa \frac{(T_s - T_1)}{\Delta z_1} \quad (7)$$

(7) Soil-moisture redistribution (Richard's equation):

$$\frac{\partial \theta}{\partial t} = \frac{\partial}{\partial z}\left[\frac{D(\theta)\partial \theta}{\partial z} + K(\theta)\right] - S_{ET} \quad (8)$$

Here R_n is net radiation; H, LE, and G are the sensible, latent, and ground heat fluxes (W/m²); α and ε are surface albedo and emissivity; σ is the Stefan-Boltzmann constant; S and L are downward shortwave and longwave radiation (RRTMG,[21]); ρ is air density; $c_p = 1004\ J/kgK$; $L_v = 2.5 \times 10^6\ J/kg$; C_h and Cq are the surface exchange coefficients

for heat and moisture; |U|, T_a, q_a are the wind speed, temperature, and specific humidity at the lowest model level; T_s and q_s are skin temperature and saturation specific humidity; r_s and r_s ,min are stomatal and minimum stomatal resistance; LAI is the leaf area index; F1–F4 are dimensionless stress functions of solar radiation, vapor-pressure deficit, air temperature, and root-zone soil moisture θ respectively; κ is soil thermal conductivity; T_1 and Δz_1 are the temperature and thickness of the first Noah soil layer; θ is volumetric soil moisture; D and K are the soil-water diffusivity and unsaturated hydraulic conductivity (Clapp–Hornberger formulation,[23]); and S_{ET} is the root-zone water-uptake sink term.

FRC_URB does not appear explicitly in any of equations (2-8). Instead, every equation is solved twice within each grid cell once over the impervious fraction by SLUCM and once over the vegetated fraction by Noah LSM, and the cell-scale composite is the area-weighted sum (equations 9-10 of section 3.2.4). Equation (5) carries the strongest FRC_URB dependence, because the moisture-availability factor in q_s approaches zero over impervious surfaces, making the cell-scale LE approximately proportional to (1−FRC_URB). The Bowen ratio β = H/LE used as a key diagnostic in Section 4.3.1 follows directly from this partitioning, and the day–night asymmetry analyzed in Section 4.3 is a direct consequence of equations (5) and (7) operating with opposite signs in the two regimes.

The simulation period covers 21 June 2025 12:00 UTC to 23 June 2025 00:00 UTC, a total of 36 h. The summer solstice provides the annual peak of shortwave forcing, ensuring that UHI and greening signals are evaluated under maximum thermal forcing and well-developed diurnal mixing. The first 12 h serve as model spin-up and are excluded from analysis, leaving a full diurnal cycle (22 June 2025, 00:00-24:00 UTC) for scenario comparison. ERA5 reanalysis at 0.25° horizontal resolution [42], [36] provides initial and lateral boundary conditions across 37 pressure levels.

3.2.4. Urban canopy scheme and the role of FRC_URB

SLUCM is activated for all urban grid cells. Each grid cell is split between an impervious (urban canopy) fraction FRC_URB and a vegetated fraction (1−FRC_URB) handled by Noah LSM. The grid-cell composite skin temperature and sensible heat flux are area-weighted combinations:

$$Ts = FRC_{URB} \times Ts(impervious) + (1 - FRC_{URB}) \times Ts(vegetation) \quad (9)$$

$$SH = FRC_{URB} \times SH(impervious) + (1 - FRC_{URB}) \times SH(vegetation) \quad (10)$$

Reducing FRC_URB increases the vegetated fraction, raising LE and lowering T_s. All greening scenario modifications were applied exclusively to the High-Density Residential

column of URBPARM.TBL (Section 3.4), since inspection of the WRF default land-use data confirmed that this is the only active urban subclass within the Ulaanbaatar D04 domain.

3.3. Model settings

The simulation period is a 36-hour window centered on the summer solstice, June 22, 2025. This was done to get the most solar forcing and make it easier to see land-surface signals when the sky is clear. D04 solves Ulaanbaatar at a horizontal resolution of 1 km, using initial and lateral boundary conditions from ERA5 reanalysis [42], [36]. We used SLUCM (sf_urban_physics=1) to show the urban canopy. This treats the urban surface as a uniform two-dimensional street canyon, which is a good balance between physical realism and computational cost for Ulaanbaatar's mostly low to medium-rise buildings. The multi-layer BEP and BEP+BEM schemes were not used.

The WRF default MODIS-IGBP land-use classification used for the D04 domain is a big problem. Inspection of URBPARM.TBL (Appendix B) using ncview confirmed that all urban grid cells within UB are assigned to a single urban class high-density residential with a uniform FRC_URB value of 0.90(CTRL). The SLUCM framework has categories for low-density residential and commercial/industrial areas, although the default WRF land-use data does not have these categories. Because of this, all changes to the greening and de-greening scenarios were only made to the High-Density Residential column of URBPARM.TBL. The geographical complexity of Ulaanbaatar's actual urban fabric, which consists of discrete commercial, apartment-block, and ger-district geometries with varying building heights, albedos, and impervious fractions, is thus depicted as a singular homogeneous urban class. This gives us a tidy way to test the first-order effect of FRC_URB, but it doesn't show how different the subclasses are in the real city.

These limitations point to clear directions for future research: multi-year simulations across seasons; combined greening–albedo experiments; inclusion of low-density residential and commercial urban classes using updated land-use datasets; and a mosaic approach to represent vegetation patch shapes. Soil-moisture sensitivity, identified as a critical control on the realized cooling potential of urban greening in semi-arid climates [1], [24], is not addressed here because of computational cost; this is a primary direction for future research (Section 5.3).

3.3.1. Domain configuration

WRF v4.6.0 [10] was configured with four one-way nested domains centered on the Ulaanbaatar synoptic station (47.92 °N, 106.85 °E), telescoping from the synoptic scale (D01, Δx = 27 km) down to the urban-microclimate scale (D04, Δx = 1 km) using a 1:3:3:3 nesting ratio (Fig. 6).

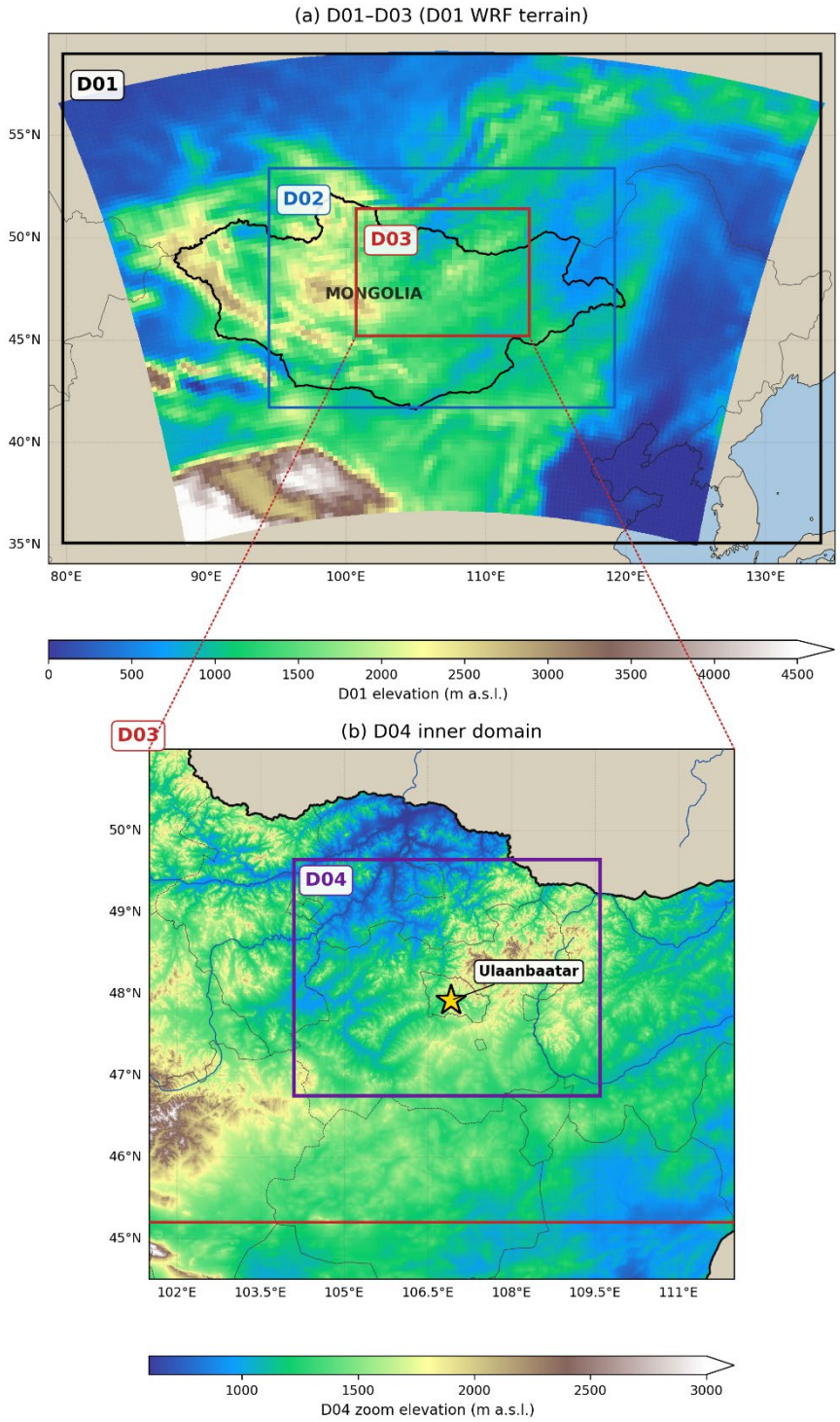


Figure 6. WRF nested domain configuration: (a) D01–D03 over East and Central Asia with D01 model terrain; (b) D04 zoom over Ulaanbaatar with high-resolution DEM.

All four domains share 40 terrain-following hybrid sigma-pressure vertical levels with the model top at 50 hPa, providing a vertical resolution of approximately 30 m near the surface. The total computational mesh comprises 214,857 horizontal cells (8,594,280 prognostic 3D grid points), of which approximately 55% lie within D04 (Table 4). Land use was initialised from the MODIFIED_IGBP_MODIS_NOAH classification (61 categories).

The D01 time step was 60 s (= 2.22 s/km), with nested-domain time steps scaled by the nesting ratio (20, 6.7, and 2.2 s for D02–D04), satisfying the CFL stability criterion at all resolutions. A single 36-h simulation required approximately 51 h of wall-clock time on the available HPC platform; the full sensitivity experiment of four simulations therefore consumed approximately 204 h (8.5 days) of cumulative integration. This computational expense, dominated by the 1-km inner domain, is the principal reason for restricting the present analysis to a single representative summer day and to a four-scenario FRC_URB sweep.

Table 4. WRF nested domain configuration

Domain	x × y × z	Horizontal cells	3D cells	Δx (km)	Coverage (km × km)
d01	121 × 91 × 41	10,800	432,000	27	3240 × 2430
d02	181 × 136 × 41	24,300	972,000	9	1620 × 1215
d03	280 × 220 × 41	61,101	2,444,040	3	837 × 657
d04	385 × 310 × 41	118,656	4,746,240	1	384 × 309
Total	-	214,857	8,594,280	-	-

3.3.2. Control run

The Control simulation (CTRL) uses FRC_URB = 0.90 for the High-Density Residential class throughout the D04 domain, representing the current urban land-use state of Ulaanbaatar. All physical parameters building height, street width, roof albedo, and anthropogenic heat was held at their default WRF URBPARM.TBL values. The first 12 h of each simulation are excluded as spin-up, and the analysis is conducted on the subsequent 24-h period covering a complete diurnal cycle (22 June 2025 00:00 UTC to 23 June 2025 00:00 UTC).

3.4. Urban greening scenarios

Four simulations were designed by modifying FRC_URB in the High-Density Residential column of URBPARM.TBL. All other parameters were held constant, ensuring that differences between simulations are attributable solely to changes in vegetation fraction. The scenarios bracket the full physically plausible range from fully impervious (FRC_URB = 1.0) to strongly greened (FRC_URB = 0.1).

Table 5. Urban Greening Scenario definitions.

Scenario	FRC_URB	Green Coverage	Description
Greening 0 % (NOGR)	1.00	0 %	Full impervious - no vegetation (reference upper bound)
Control (CTRL)	0.90	10 %	Baseline - current Ulaanbaatar conditions
Greening 50 % (GR50)	0.50	50 %	Moderate greening - equal urban/vegetated fractions
Greening 90 % (GR90)	0.10	90 %	Maximum greening - 10% impervious

The original assignment sheet proposed greening levels of 20%, 40%, and 60%. The present study expanded this range to 0%, 10%, 50%, and 90% to capture the full physically meaningful spectrum: a fully built-up reference, the existing dense built-up structure of Ulaanbaatar (retained as CTRL), an intermediate scenario bracketing the original midpoint, and a strongly greened scenario testing the response near the vegetation-dominated limit. This wider range proved essential for revealing the non-monotonic T2 response in the UB cell identified in Section 4.3.4, which would not have been visible at the original 20-60% bracket. Sensitivity to vegetation type and to soil moisture, also originally proposed in the assignment sheet, was deferred to future work because of the high computational cost of each WRF simulation; This is detailed in Section 5.3.

3.5. UHI calculation and analysis method

The Urban Heat Island intensity is computed as the simulated 2m air temperature difference between the urban grid point at Sukhbaatar Square and the mean of three rural reference points (Fig. 7, Table 6). Following the convention of Oke [2], the UHI is defined as

$$UHI(t) = T_{2,urban(t)} - \overline{T_{2,rural\ (t)}} \quad (11)$$

Where the rural mean is

$$T_{2,rural\ (t)} = \frac{1}{3}\sum_{k=1}^{3} T_2, k(t)\ \text{, k=1,2,3} \quad (12)$$

Three rural reference points (Fig. 7) were selected following Stewart and Oke [43]: (i) absolute elevation difference within ±50 m of UB center to remove orographic adiabatic contamination; (ii) non-urban MODIS-IGBP land-use class to ensure Noah LSM controls the rural surface response; (iii) distance 8-35 km from the urban core to lie outside the UHI advection plume; and (iv) distribution across cardinal sectors to avoid over-representing any single drainage direction. Among the candidate cells satisfying these criteria, the three selected points are Takhilt (W, ΔHGT=−1 m), Buyant-Ukhaa (SW, ΔHGT= −2 m), and Officer (E, ΔHGT=15 m). All three share the MODIS-IGBP grassland land-use class (LU=10) and lie within the 1301-1318 m elevation band, ensuring a (Table. 7)homogeneous rural background (Table 6). Buyant-Ukhaa coincides with the long-term observation station used by Ganbat et al. [5] in their 31-year UHI climatology, providing a direct link to the canonical observational dataset for UB.

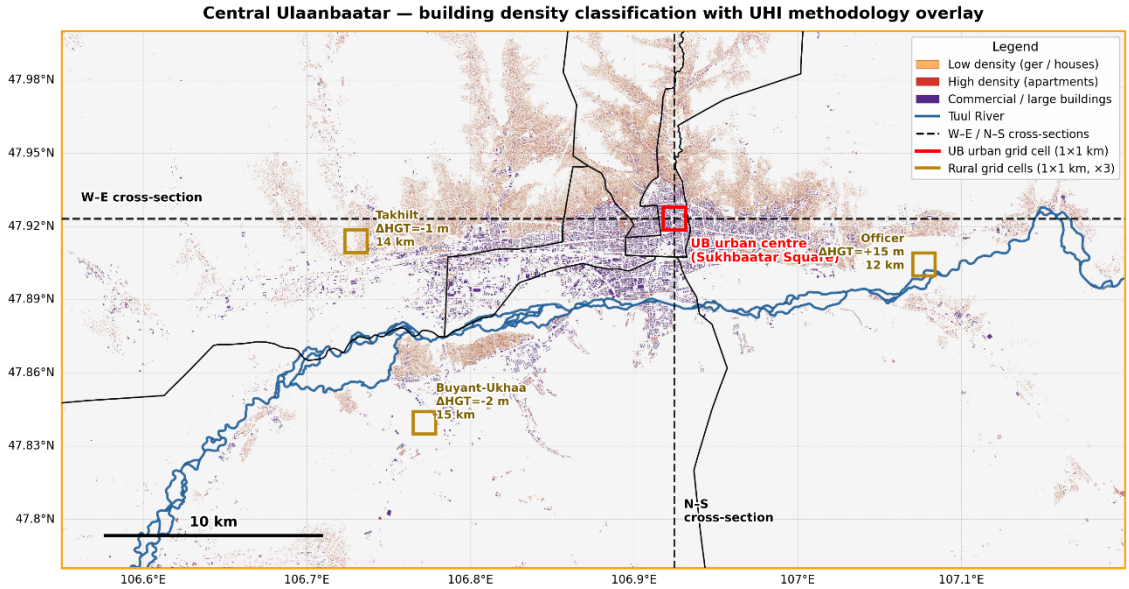


Figure 7 Spatial framework for the UHI calculation

Table 6. Coordinates and characteristics of the urban grid point and three rural reference points used in the UHI calculation

Point	Lat (°N)	Lon (°E)	HGT (m)	ΔHGT vs UB (m)	LU class	Distance from UB (km)	Direction
Ulaanbaatar center	47.92	106.92	1303	-	13 (urban)	-	-
Takhilt	47.91	106.73	1302	-1	10(grassland)	14	W
Buyant Ukhaa	47.84	106.77	1301	-2	10 (grassland)	15	SW
Officer	47.90	107.08	1318	15	10 (grassland)	12	E

3.6. Output variables diagnosed

The following prognostic and diagnostic variables are extracted from the WRF output files at hourly intervals over the D04 domain and (Table 8)used for scenario comparison (Table 7). Vertical cross-sections, plan-view maps, and Skew-T diagrams (Fig. 9-17) are produced using Python (matplotlib, netCDF4, scipy, and MetPy).

Table 7. Output variables diagnosed from WRF simulations.

Variable	WRF name	Unit	Physical meaning
2 m air temperature	T2	K to °C	Primary UHI / greening diagnostic
Surface skin temperature	TSK	K	Direct output of SLUCM / Noah composite
Sensible heat flux	HFX	W/m²	Heating of boundary-layer air
Latent heat flux	LH	W/m²	Evapotranspiration signal
Ground heat flux	GRDFLX	W/m²	Subsurface storage term
Downward shortwave radiation	SWDOWN	W/m²	Incident solar forcing
Outgoing longwave radiation	OLR	W/m²	Surface radiative loss (nighttime)
Soil moisture (layer 1)	SMOIS(1)	$m^3\ m^{-3}$	Water availability for evapotranspiration
Planetary boundary-layer height	PBLH	m	Mixing-depth response
Terrain elevation	HGT	m a.s.l.	Used for 3D visualisation
Land-use index	LU_INDEX	-	Identifies urban cells (code 13 = HD residential)

Scenario difference fields ΔX = X(scenario)─X(CTRL) are calculated cell-wise for each output variable and displayed as 2-D maps and vertical cross-sections. Chapter 4's scenario inter-comparison relies on domain-averaged diurnal cycles of H, LE, T2, and TSK in urban cells.

4. Results and Discussion

4.1. Validation against radiosonde observations

To establish the credibility of the simulated land–atmosphere response analyzed in Sections 4.2 and 4.3, the WRF CTRL profile was validated against the two operational radiosonde launches at WMO station 44292 (Ulaanbaatar) during the analysis period: 12 UTC 22 June (= 20 LST) and 00 UTC 23 June (= 08 LST). Both soundings were retrieved from the University of Wyoming Radiosonde Archive [44]. The comparison is shown in Figure 8 with layer-mean RMSE and bias annotated on each panel.

The simulated temperature profile reproduces the observed structure to within 1.19°C RMSE at 20 LST and 1.7°C RMSE at 08 LST, with overall warm biases below 0.7°C. The mid-tropospheric agreement is exceptional, with T RMSE of only 0.3°C at 20 LST and 0.3°C at 08 LST in the 500-700 hPa layer, confirming that the imposed ERA5 boundary conditions are well represented. These values fall comfortably within the acceptance range routinely reported for mesoscale WRF simulations: Diaz et al. [45] reported an overall potential-temperature RMSE of 2.3°C in subtropical Brazil, and Muñoz et al. [46] reported tropical-Andes T RMSE values below 1°C. The present simulation therefore meets and, in the mid-troposphere, considerably exceeds these published benchmarks.

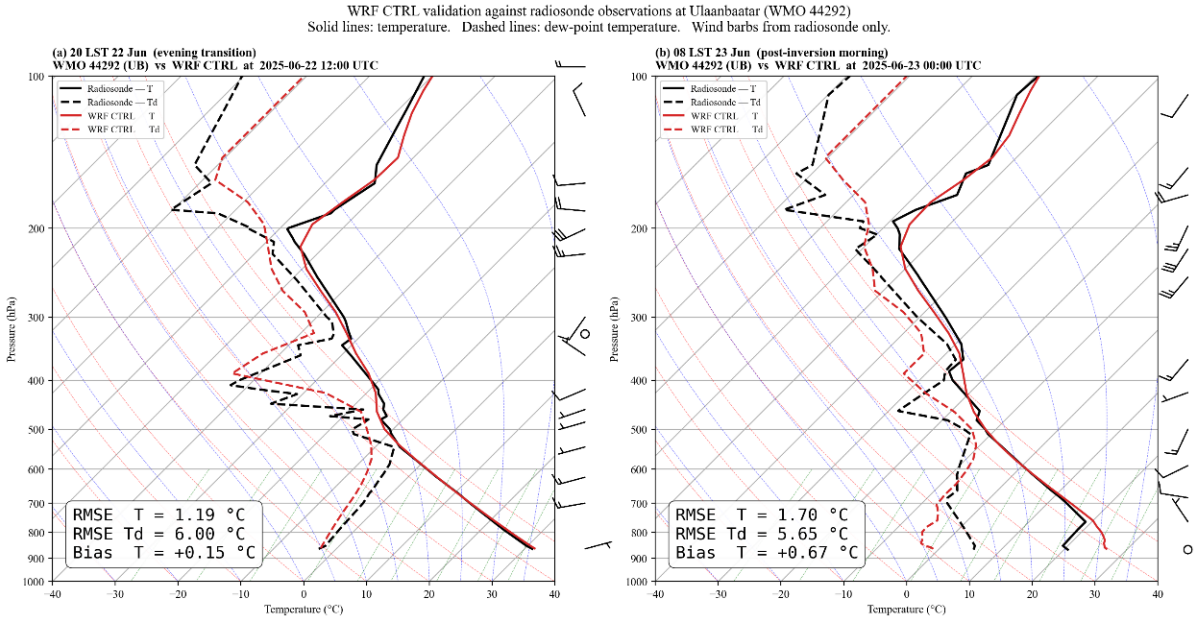


Figure 8 WRF CTRL (red) versus radiosonde (black) at WMO station 44292 (Ulaanbaatar) for (a) 20 LST 22 Jun (12 UTC, evening transition) and (b) 08 LST 23 Jun (00 UTC, post-inversion morning). Solid lines show temperature, dashed lines show dew-point temperature;

The only notable deviation occurs at 700–900 hPa at 08 LST, where the simulated CTRL underestimates the strength of the observed surface inversion by approximately 2.5°C (T RMSE=3.4°C, warm bias=2.6°C). This well-documented limitation of mesoscale models in resolving deep nocturnal inversions [6], [11] implies that the simulated nocturnal greening response analyzed in Section 4.3.4 is, if anything, a conservative lower-bound estimate of the true magnitude of the basin-scale physical processes at work. The Td RMSE of 5.65-6.00°C across the full troposphere is dominated by the upper troposphere; in the 700-900 hPa layer, Td RMSE drops to 1.5°C at 20 LST, comparable to the moisture skill reported by Diaz et al. [45]. The validation confirms that WRF CTRL supports the FRC_URB sensitivity analysis with high fidelity.

4.2. Control run

Figure 9 shows two cross-sections of the 24-h mean T2 and terrain elevation through Ulaanbaatar on 22 June 2025. Panel (a) is the west–east transect along 47.92°N, and panel (b) is the north–south transect along 106.90°E. In both, the left axis shows T2 (red, orange, and blue lines for the 24-h, daytime, and nocturnal means); the right axis shows terrain elevation (brown); and the lower bars indicate urban (grey, FRC_URB = 0.90) and rural (green) grid cells.

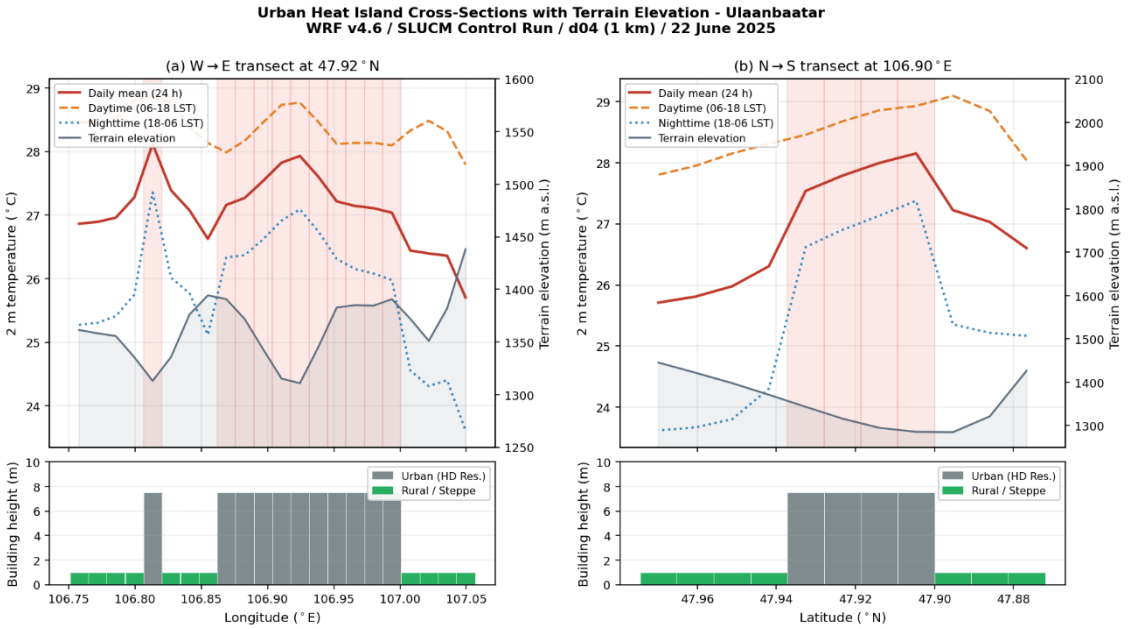


Figure 9 (a) West–east and (b) north–south cross-sections of T_2 and terrain elevation through UB on 22 June 2025.

The west–east transect (a) reveals the classic valley-floor UHI signature. Terrain is relatively flat (1300–1380 m) along the Tuul River corridor, and within the continuous urban cluster, the 24h mean T2 reaches 27-28°C, roughly 2°C warmer than the rural pixels at both ends, consistent with the observed summertime UHI of 2.5°C [5]. The north–south transect (b) exposes the topographic constraint of Bogd Khan Uul: terrain rises from 1320 m in the northern valley to over 1600 m at the southern boundary, and T2 falls by 3°C across the same gradient. The urban cluster sits in the center of the transect and produces a localized maximum superimposed on the topographic gradient. Together, the two panels confirm that WRF/SLUCM correctly identifies the urban land surface as the dominant local control on near-surface temperature.

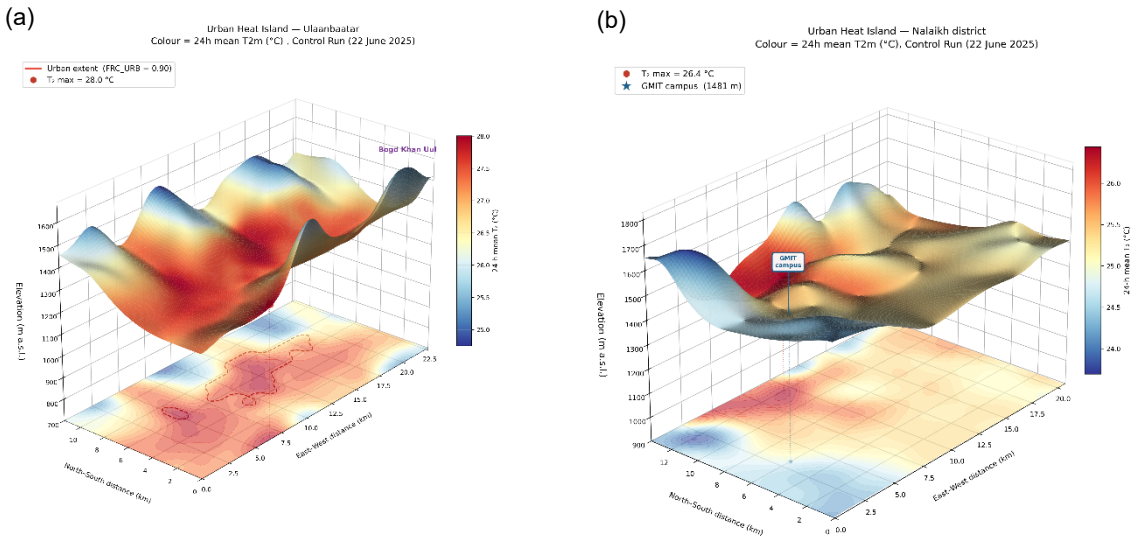


Figure 10 3D terrain of (a) Ulaanbaatar and (b) Nalaikh domain (D04, 1 km) with T2M projection. Red contour on terrain = urban extent (FRC_URB = 0.90).

Figure 10 presents the three-dimensional terrain surfaces of the Ulaanbaatar urban core (panel a) and the Nalaikh satellite district (panel b), colored by the 24h mean T2 simulated by the control run on 22 June 2025. Both subdomains are extracted from the innermost WRF grid (D04, 1 km) under identical synoptic forcing from ERA5; the only difference between them is their land-surface configuration. Panel (a) is dominated by high-density residential urban cells (FRC_URB=0.90), while panel (b) contains only scattered urban cells and is primarily classified as grassland in the MODIS-IGBP land-use dataset. The GMIT campus (47.7706°N, 107.2439°E, 1481m a.s.l.) is marked as a spatial reference in panel (b). The vertical axis is exaggerated 15× to make the valley–slope morphology visible; horizontal axes are in true kilometers; and the floor plane projects the T2 field for direct comparison with the terrain above.

Table 8. Summary statistics of the control-run T2 field in the two sub-domains (24-hour mean, 22 June 2025).

Property	Ulaanbaatar box	Nalaikh box
Longitude range	106.75-107.05°E	107.20-107.48°E
Latitude range	47.87-47.97°N	47.72-47.84°N
Elevation range	1250-1650	1350-1800
T2 minimum (°C)	24.9	23.9
T maximum (°C)	28.0	26.4
TM range (°C)	3.1	2.5
Dominant land use	High-density residential	Grassland / sparse residential
FRC_URB	0.90	default non-urban

The Ulaanbaatar panel reveals the canonical dome-like UHI signature first documented [5] and reproduced numerically by Ganbat & Baik [6]. The valley floor between Bogd Khan Uul (south) and the Khentii foothills (north) exhibits the warmest 24-h mean values,

reaching 28°C within the high-density urban contour and declining by 3°C toward the surrounding mountain slopes. The Nalaikh panel shows a markedly different pattern: T2 ranges only from 23.9°C to 26.4°C, 1.6°C cooler than the Ulaanbaatar maximum despite the two sites being separated by less than 40 km. The 1.6°C contrast quantifies, in a single clear-sky summer snapshot, how strongly Ulaanbaatar's current urban fabric elevates local T2 relative to a nearby less-urbanized site.

4.3. Effect of urban greening

4.3.1. Surface energy balance

The day-night asymmetry analyzed in Section 4.3 originates in the surface energy-balance partitioning. Figure 11 shows the 24h time series of sensible heat flux (HFX), LH, β = H/LE, TSK, PBLH, and RH_2 averaged over the urban analysis box (106.75–107.05°E, 47.87–47.97°N) for the four FRC_URB scenarios; day-mean and night-mean values are summarized in Table 9.

Table 9. Daytime (06-18 LST) and night-time (18-06 LST) means of the urban-box surface energy balance for the four FRC_URB sensitivity simulations on 22 June 2025.

Period	Greening	HFX (W/m^2)	LH (W/m^2)	Bowen	TSK (°C)	PBLH (m)	RH2 (%)
Day (06-18 LST)	NOGR	166.1	78.8	1.59	36.60	2169	16.8
	CTRL	163.1	82.5	1.50	36.51	2163	16.3
	GR50	157.8	98.8	1.22	36.28	2158	17.1
	GR90	153.8	114.4	1.03	35.98	2145	16.9
Night (18-06 LST)	NOGR	-6.8	10.3	0.45	21.07	727	23.3
	CTRL	-7.7	10.3	0.38	20.90	684	22.3
	GR50	-9.2	12.0	0.22	20.53	753	23.9
	GR90	-9.3	13.1	0.13	20.12	653	23.6

The Bowen ratio is the cleanest diagnostic of greening intensity (Fig. 11c). Increasing the greening fraction from 0% to 90% reduces the daytime β from 1.59 to 1.03, a 35% reduction. At night β decreases more dramatically, from 0.45 (NOGR) to 0.13 (GR90), reflecting the suppression of upward H as the surface cools relative to the air. This systematic ordering arises from the SLUCM partitioning of net radiation: vegetation cover provides the only available ET channel in the model, and FRC_URB directly controls the fraction of each grid cell that participates.

LE shows a near-monotonic increase with greening fraction (Fig. 11b, Table 9). The 24h daytime mean rises from 78.8 W/m^2 (NOGR) to 114.4 W/m^2 (GR90), a 45% increase. After sunset all four scenarios converge to LE = 10-13 W/m^2 as plant stomata close and bare-soil evaporation diminishes; inter-scenario differences shrink to <1<3W/m^2. This nocturnal collapse of the latent signal explains why the substantial daytime moisture

benefit (ΔTd up to 1.7°C; Section 4.3.3) is not sustained through the night (ΔTd≤0.3°C; Section 4.3.4). HFX shows the inverse pattern but a much smaller relative response (Fig. 11a): the daytime mean decreases from 166.1 W/m^2 to 153.8 W/m², only 7%. This asymmetry, a 45% increase in LH balanced by only a 7% decrease in HFX, reflects the SLUCM closure: net radiation is largely conserved while the partitioning shifts toward the latent pathway.

TSK responses are larger than T2 responses (Fig. 11d). The daytime means TSK contrast between 0% and GR90 greening is 0.6°C (36.6 vs. 36°C), approximately three times larger than the corresponding ΔT2 of 0.2°C (Section 4.3.4). The discrepancy reflects the thermal decoupling between the radiating surface and the deep daytime mixed layer (PBLH 2.2 km; Fig. 11e), which efficiently dilutes the surface signal before it reaches the 2m level. This is consistent with the global synthesis of Hao et al. [24] and indicates that infrastructure-level adaptation strategies (cool roofs, light pavements, and shaded surfaces) targeting TSK may yield substantially larger thermal benefits than a T2-based analysis alone would suggest.

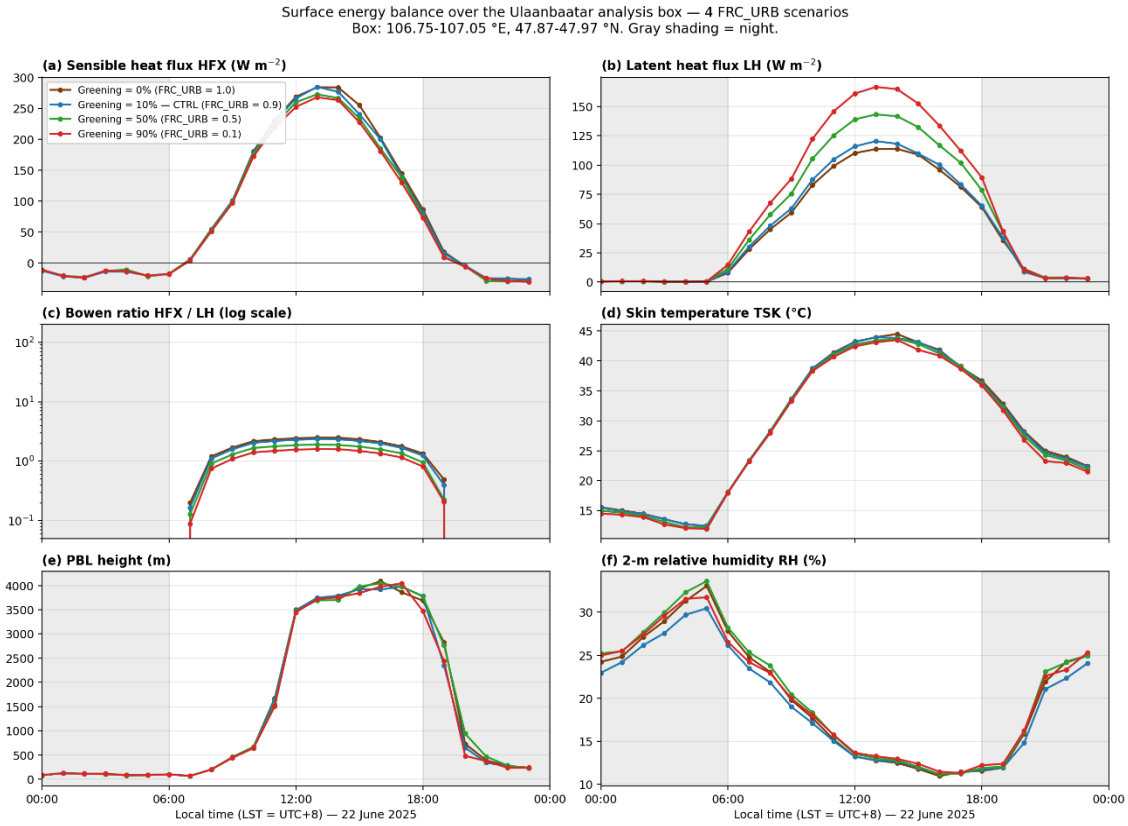


Figure 11 The surface energy balance for the Ulaanbaatar urban analysis box (106.75-107.05 °E, 47.87-47.97 °N) in the four FRC_URB sensitivity simulations on 22 June 2025 includes sensible heat flux (HFX), latent heat flux (LH), Bowen ratio (β = HFX / LH on a logarithmic vertical scale), skin temperature (TSK), PBL height, and 2-m relative humidity. The four possibilities are: NOGR (FRC_URB = 1.0, brown), 10% (CTRL, FRC_URB = 0.9, blue), 50% (0.5, green), and 90% (0.1, red). Grey represents night (18-06 LST).

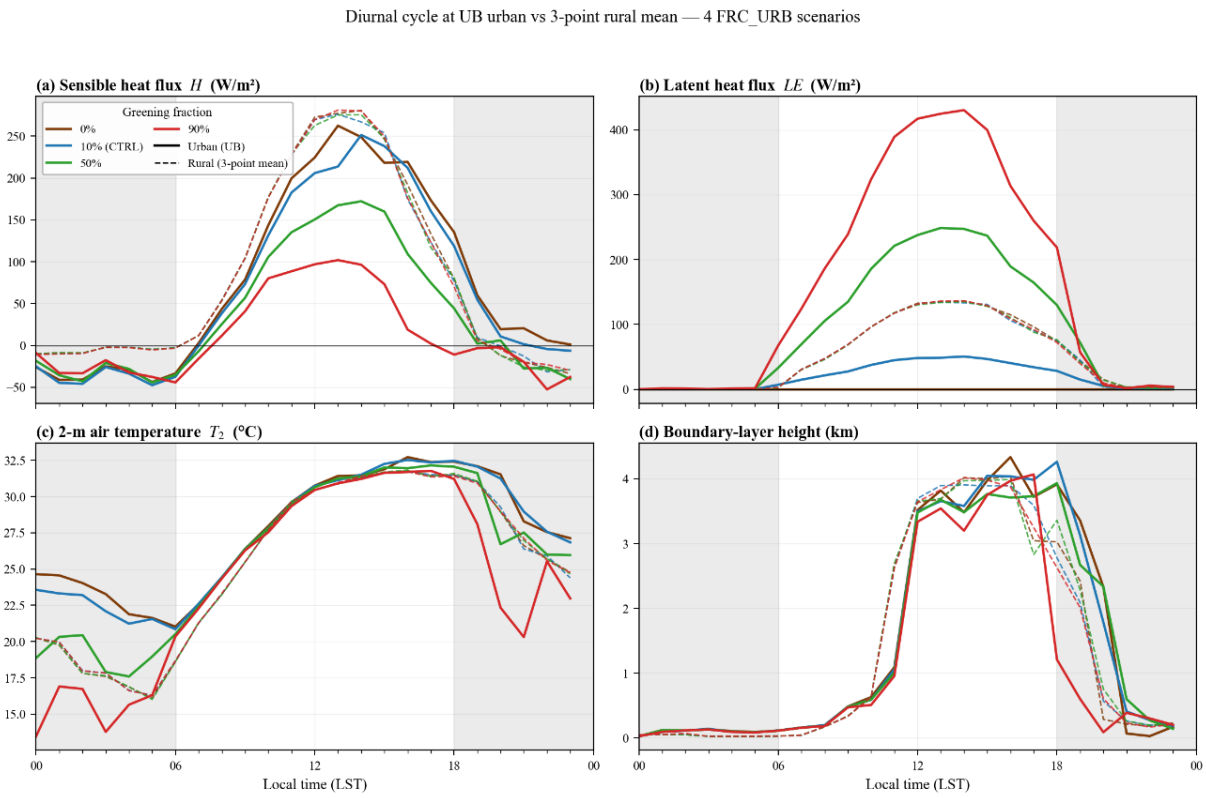


Figure 12 Diurnal cycle of the simulated surface energy balance and boundary-layer state at the Ulaanbaatar urban centre (solid lines) and the 3-point rural reference mean (dashed lines) for the four FRC_URB scenarios on 22 June 2025: (a) sensible heat flux H, (b) latent heat flux LE, (c) 2m air temperature T2M, and (d) boundary-layer height. Line colours indicate the four greening scenarios; gray shading marks the night period (18-06 LST).

Figure 12 complements the box-mean analysis by decomposing the same variables into the urban grid point at the Ulaanbaatar center (solid lines) and the corresponding 3-point rural reference mean (dashed lines). The urban–rural contrast confirms the box-mean findings: the rural reference fluxes are essentially identical between scenarios since all three rural points are vegetated, while the urban fluxes reorganize systematically with FRC_URB. The mid-day urban LE rises from near zero in the densely built configuration to over 400 W/m^2 in the strongly greened configuration, with the corresponding HFX falling from 260 to 100 W/m^2. T2 shows a much smaller spread, again confirming the thermal decoupling between the radiating surface and the well-mixed convective boundary layer.

4.3.2. Greening sensitivity

This section examines the simulated response of the lower troposphere over Ulaanbaatar to systematic modification of the urban fraction at two contrasting times of day: the afternoon convective peak (14 LST = 06 UTC, 22 June) and the deep nocturnal stable layer (05 LST 23 June = 21 UTC 22 June). The four sensitivity simulations' vertical profiles for both snapshots are compared in Figure 13, and Table 11 summarizes the surface-level values.

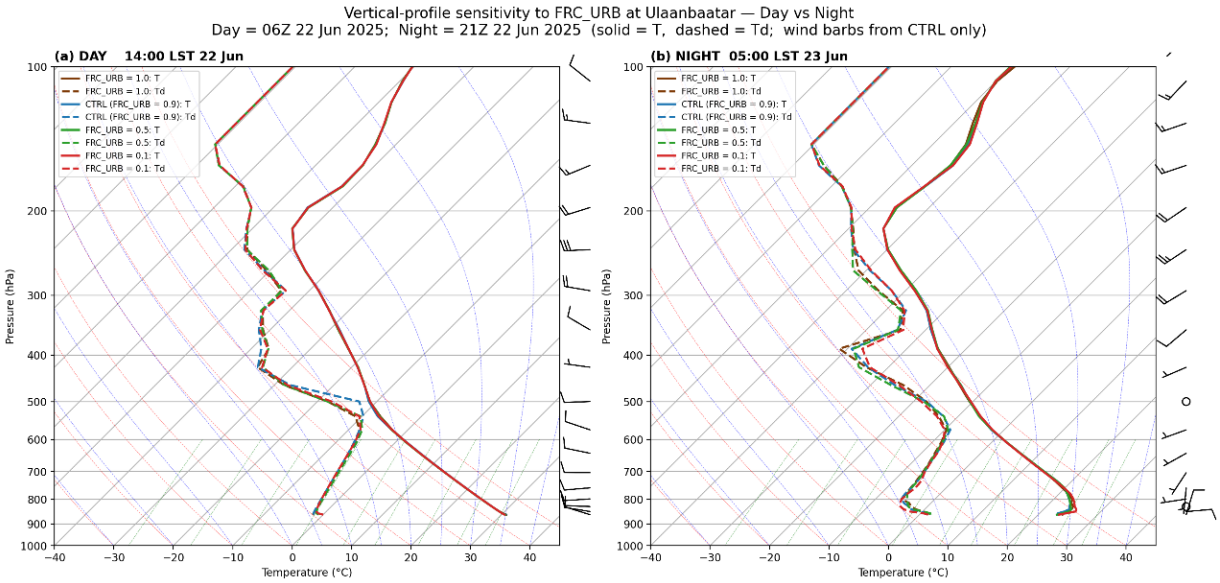


Figure 13 Comparison of simulated vertical profiles at the UB grid point in WRF d04 for four FRC_URB sensitivity simulations on 22 June 2025: (a) daytime peak at 14 LST and (b) deep nocturnal stable layer at 05 LST. Wind barbs are shown for the CTRL run only.

The full troposphere is virtually identical between the four simulations above approximately 700 hPa (Fig. 13), where the large-scale forcing imposed by the ERA5 boundary conditions dominates. The greening signal is therefore confined to the boundary layer, and its surface-level magnitude differs sharply between the daytime and night-time regimes.

Table 10. Simulated surface values (T, Td, mixing ratio QV, relative humidity RH) and differences with respect to the CTRL run at the Ulaanbaatar grid point (WRF d04) for the day and night snapshots on 22 June 2025.

Time	Greening	T (°C)	Td (°C)	QV (g/kg)	RH (%)	ΔT (°C)	ΔTd (°C)	ΔQV (g/kg)
DAY 14:00 6/22	NOGR	30.82	-1.76	3.91	12.1	0.08	-0.11	-0.03
	CTRL	30.74	-1.65	3.94	12.3	-	-	-
	GR50	30.64	-0.73	4.21	13.2	-0.10	0.92	0.28
	GR90	30.53	0.03	4.45	14.0	-0.21	1.67	0.52
NIGHT 05:00 6/23	NOGR	24.07	1.81	5.07	23.3	0.81	0.32	0.12
	CTRL	23.26	1.49	4.95	23.9	-	-	-
	GR50	23.13	1.91	5.10	24.8	-0.13	0.43	0.16

GR90	23.50	1.46	4.94	23.5	0.24	-0.03	-0.01

4.3.3. Daytime response

At 14 LST the response to greening is monotonic and consistent with the canonical ET-cooling mechanism, but its magnitude is small. Increasing the greening fraction from NOGR to GR90 lowers the surface T2 by 0.3°C (from 30.8°C to 30.5°C, Table 10), while raising the surface dew point by 1.8°C (from −1.8°C to 0.03°C) and the surface mixing ratio by 0.55 g/kg (from 3.91 to 4.45 g/kg). The corresponding rise in RH is modest in absolute terms (12.1% to 14.0%) but represents a 16% relative enhancement of the boundary-layer moisture content over the urban core. This pattern is the fingerprint of an ET-limited regime.

In the dry semi-arid summer climate of Ulaanbaatar, where surface RH falls below 15% at the daytime peak, the additional vegetation introduced by reducing the urban fraction is unable to extract enough soil moisture to drive a substantial latent flux. The water released through transpiration is rapidly mixed throughout a deep convective boundary layer (Figure 13a shows the dry-adiabatic surface layer extending up to 700 hPa, consistent with summer-afternoon mixing depths of 2.5-3 km reported by Ganbat & Baik [6]). The per-unit-volume cooling effect is therefore small, while the total moisture flux remains substantial. The dominant outcome of greening is thus atmospheric humidification rather than thermal cooling. This behavior is consistent with the global analysis of Hao et al. [24], who showed that semi-arid cities exhibit "urban wet island" effects exactly like the moisture-dominant pattern observed here for Ulaanbaatar.

4.3.4. Night-time response

At 05 LST, the simulated reaction changes direction from what is expected in a classical UHI and shows a non-monotonic reliance on FRC_URB. This is the principal finding of this study. The GR50 configuration gives the lowest surface temperature at night (T_sfc = 23.1°C, ΔT = −0.1°C compared to CTRL; Table 10). On the other hand, increasing the urban fraction toward fully built-up (NOGR, ΔT = 0.8°C) and decreasing it further toward strongly greened (GR90, ΔT = 0.2°C) both raise surface temperatures. So, the middle configuration is the real best, and CTRL is 0.1°C above this best.

Figure 14 shows vertical cross-sections through the Ulaanbaatar basin in the CTRL simulation at the same two snapshot times to highlight the spatial organization that creates this U-shape.

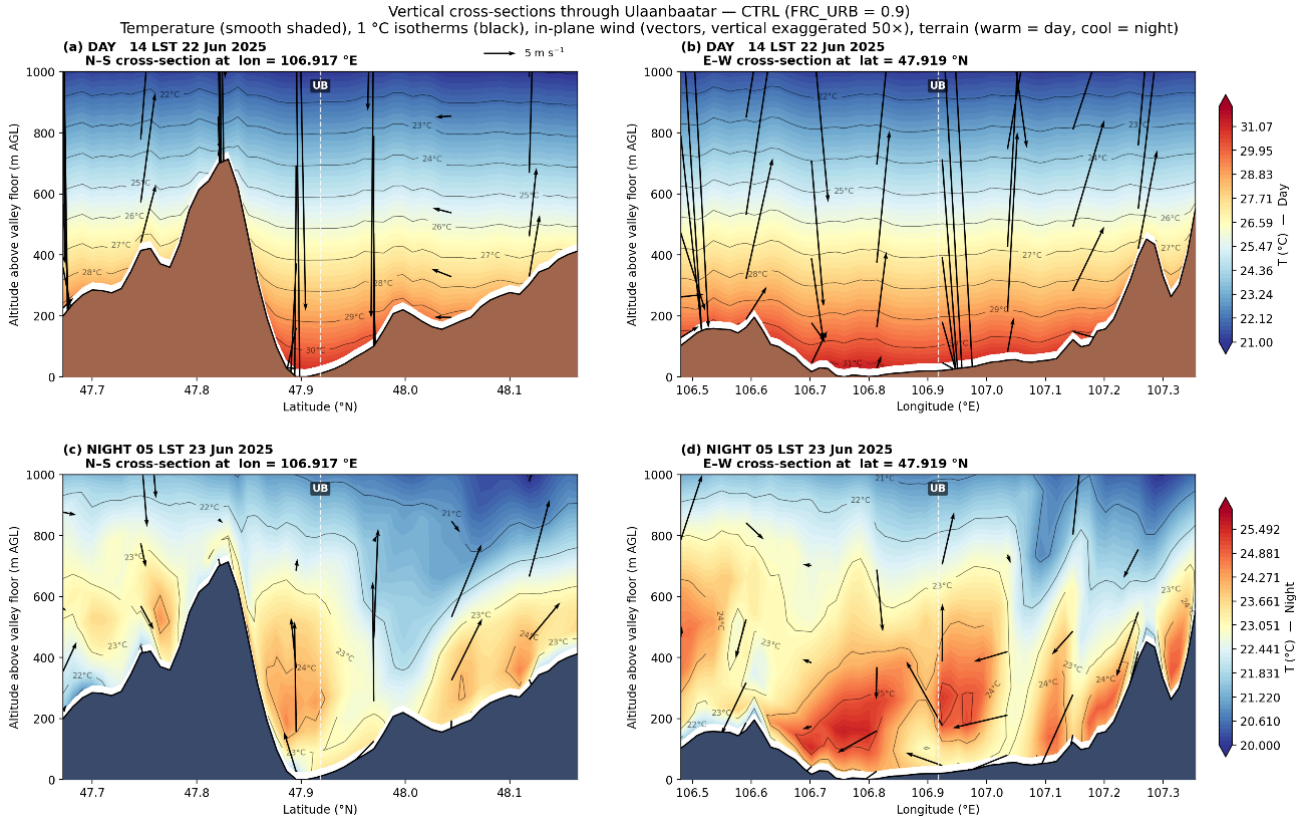


Figure 14 Day vs night vertical cross-sections through the UB basin in the CTRL simulation: N–S and E–W transects at 14 LST and 05 LST.

The night panels of Figure 14 show the classic katabatic cold-pool of the Ulaanbaatar basin that Ganbat & Baik [6] wrote about: The Khentii Nuruu (north) and Bogd Khan (south) mountains around the valley are chilly, and the air flows down their slopes and pools at the valley bottom. A warm layer, on the other hand, is confined between 200 and 400 m AGL right over the Ulaanbaatar center. Figure 13b's dew-point profile likewise clearly shows this, with a definite minimum at 800 hPa. The difference between day and night shows how uneven the Ulaanbaatar basin atmosphere is. The daytime panels show a deeply mixed convective boundary layer with nearly horizontal isotherms up to 600 m AGL and only a weak signature of the urban core at the surface. This is consistent with the small daytime ΔT values in Table 10 (≤0.3°C between NOGR and GR90).

The observed U-shape is the result of these three forces working together: a fully built-up surface releases heat storage, a strongly greened surface degrades cold pools by making them less rough, and the intermediate configuration balances these two opposing tendencies. This U-shape is a result that is only true for this basin and shouldn't be applied to all basins. In towns with flat terrain where the traditional UHI process is most important [2], [3] greening usually cools the air at night by both releasing less heat

and increasing evaporative damping, which creates a steady reaction. The non-monotonic response seen is a direct result of the significant topographic force in the Ulaanbaatar basin and the urban roughness katabatic interaction[6], [11]. The asymmetric Yangtze WRF heatwave study [47] recorded a comparable "low daytime, high nighttime" UHI/UDI asymmetry in a humid background climate, suggesting that the diurnal asymmetry is a persistent characteristic of urban–rural energy partitioning, despite the specific U-shape concerning FRC_URB seeming exclusive to basin environments.

4.3.5. Spatial structure of the response across greening scenarios

The point-based analysis in sections 4.3.3-4.3.4 shows what the main physical processes are at the Ulaanbaatar grid point. This section shows vertical cross-sections over the basin for all four sensitivity simulations at both snapshot periods (Fig. 15) to see how this reaction changes across the whole set of FRC_URB scenarios. Three structural observations arise.

The greening proportion doesn't have much of an effect on the structure of the day. The eight daylight panels all show the same well-mixed convective boundary layer. The isotherms are almost horizontal up to 600 m AGL, and the warm surface layer (T>30°C) is only found on the valley floor. There is almost no variation between the four scenarios when it comes to the position and form of the daytime thermal axis. The only consistent difference is that the peak temperature inside the urban contour goes down somewhat as the greening proportion goes up. The upslope wind component along the surrounding mountain flanks looks the same, which means that the midday mountain–valley circulation is mostly caused by terrain-driven differential heating and is not affected by the FRC_URB change the night-time panels reveal a markedly different structure. The traditional katabatic cold-pool signature, which is the warm residual layer confined between 200 and 400 m AGL above the Ulaanbaatar center, changes in a systematic way throughout the four scenarios. The FRC_URB = 1.0 configuration has the most intense and tightly packed warm pool. The peak temperatures in the core, which is directly over the Ulaanbaatar center, reach 25-26°C. As the greening fraction goes up, the warm-pool core gets weaker and wider: the CTRL run is 0.5-1°C cooler at the core than FRC_URB = 1.0; FRC_URB = 0.5 makes the warm pool wider but a little cooler; and FRC_URB = 0.1 shows the most diffuse anomaly, which has moved toward the southern half of the basin.

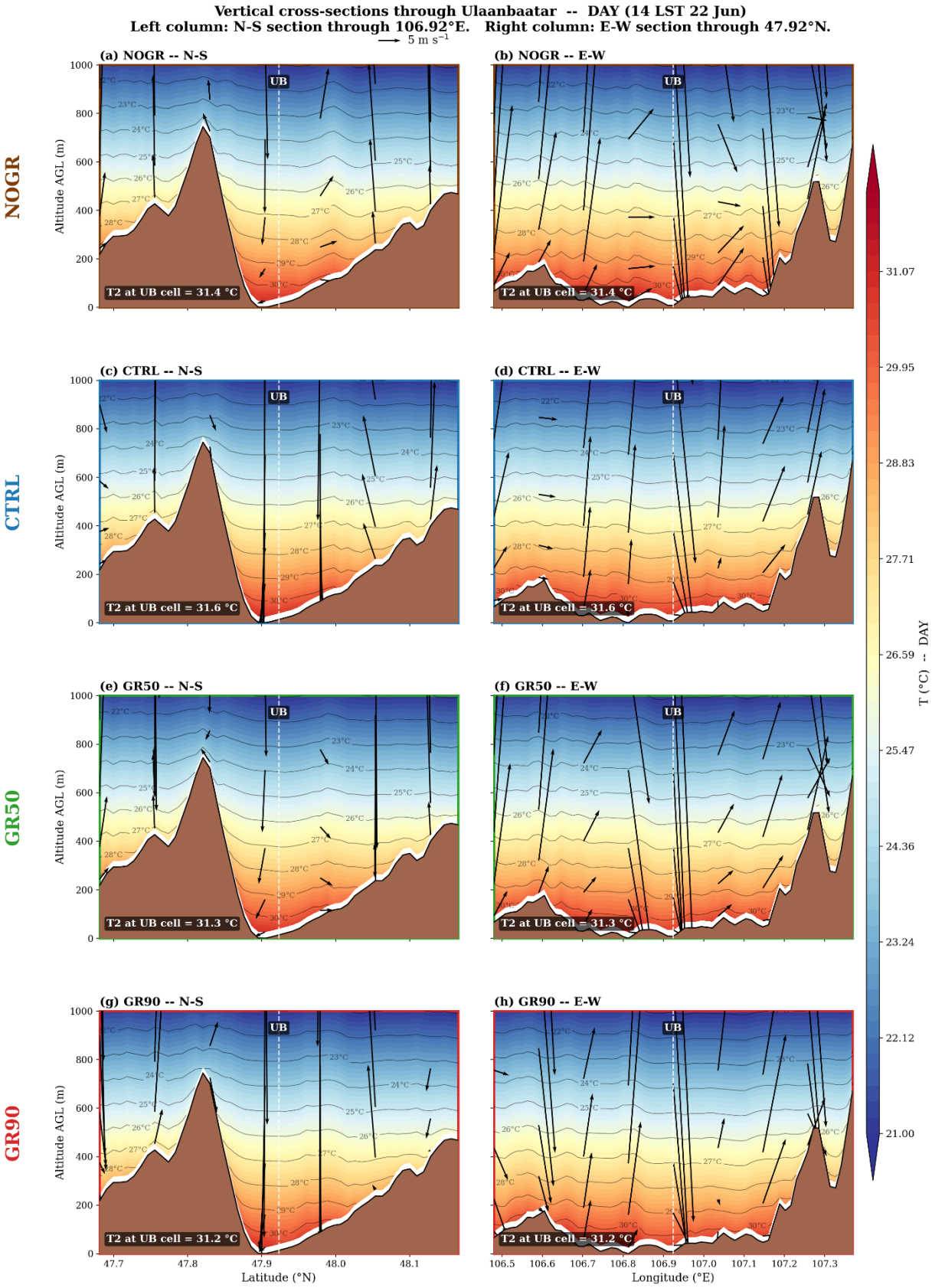


Figure 15a. Day vertical cross-sections through Ulaanbaatar for four FRC_URB sensitivity simulations on 22 June 2025.

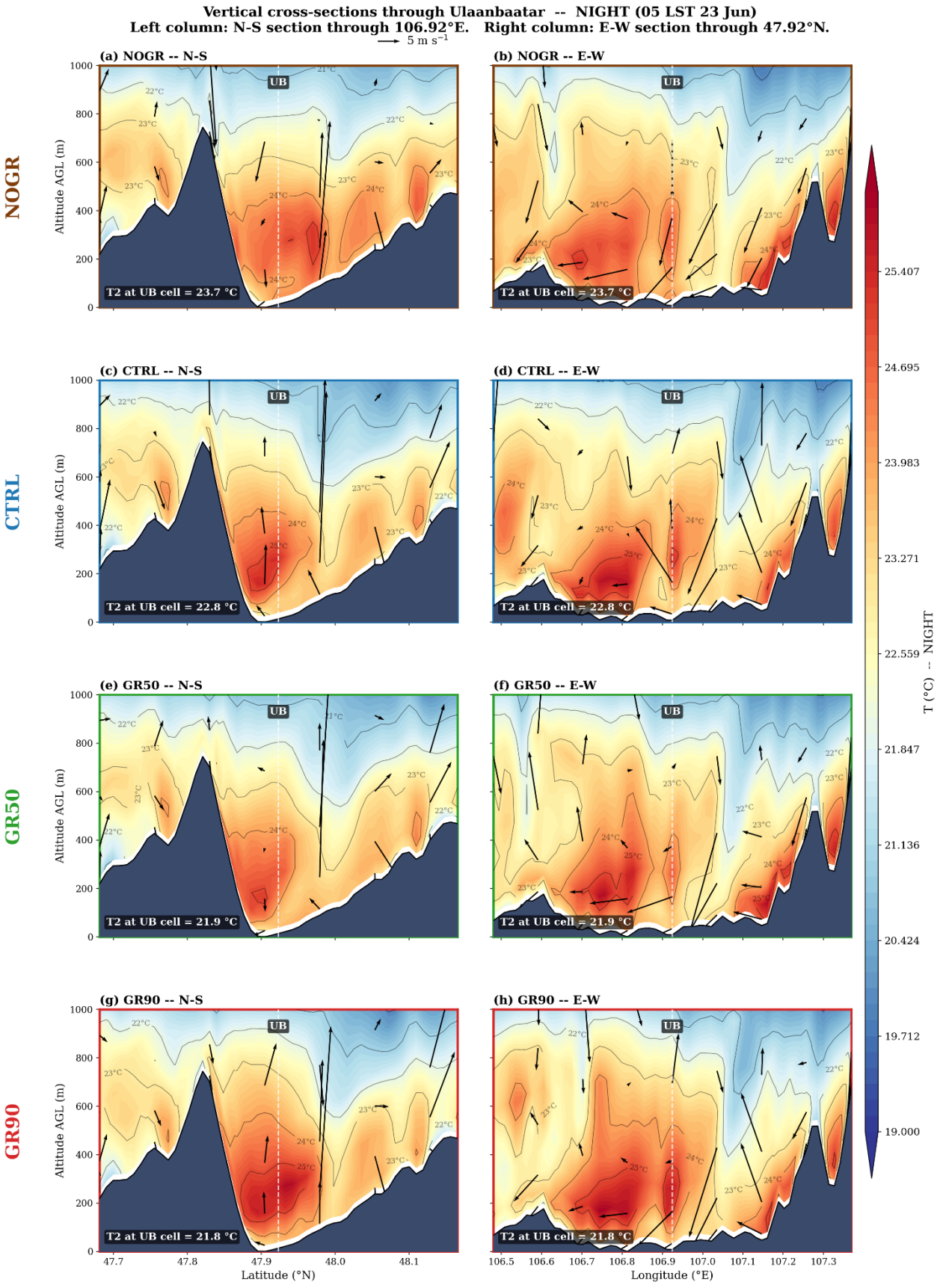


Figure 15b. Night vertical cross-sections through Ulaanbaatar for four FRC_URB sensitivity simulations on 22 June 2025.

As greening increases, the katabatic drainage flow becomes stronger in a steady way. In the nighttime N-S sections along the lower mountain flanks, wind vectors show progressively stronger downward components from FRC_URB = 1.0 to FRC_URB = 0.1. This is in line with the roughness-mediated mechanism described by [48]: a lower aerodynamic roughness over the more-vegetated surface offers less resistance to downslope drainage, which lets cold air build up more quickly along the slopes and at the base of the basin walls. The 05 LST photo, which was taken around seven hours after sunset, shows this drainage flow at its most developed level.

4.3.6. UHI intensity at Ulaanbaatar vs 3-point rural mean

The findings of section 4.3.2-4.3.5 are synthesized here as the simulated UHI intensity, computed following equation (11) as the difference between T2 at the Ulaanbaatar urban center and the mean of the three rural reference points (Takhilt, Buyant-Ukhaa, and Officer) (Fig. 7). The diurnal evolution and the day-mean and night-mean values as a function of greening fraction are shown in Figure 16.

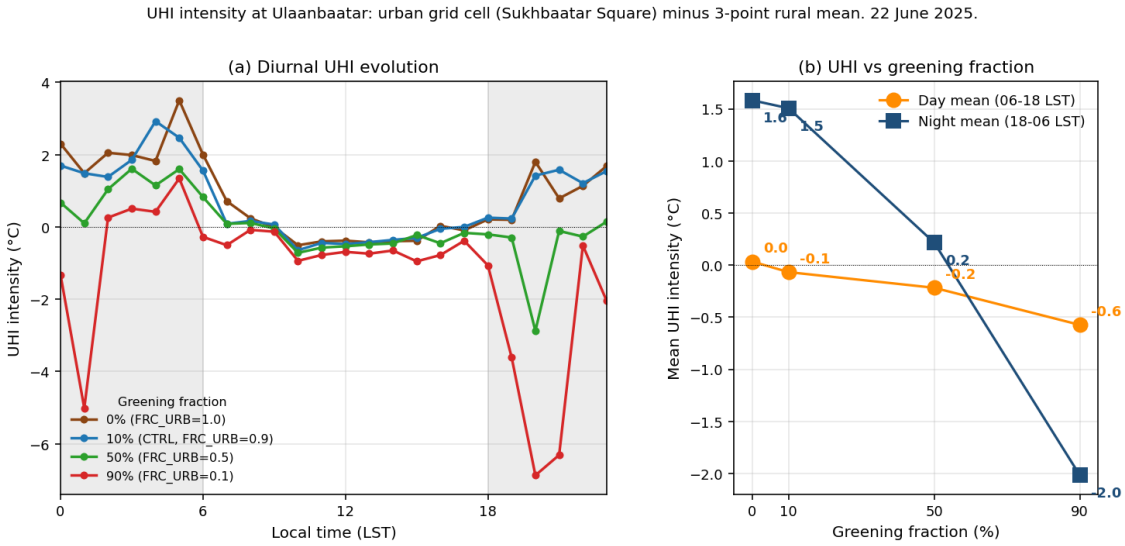


Figure 16 Urban Heat Island intensity at Ulaanbaatar (UB grid cell minus mean of 3 rural grid cells: Takhilt, Buyant-Ukhaa, and Officer) on 22 June 2025: (a) hour-by-hour diurnal evolution for the four FRC_URB scenarios; (b) day-mean (06–18 LST, orange circles) and night-mean (18–06 LST, blue squares) UHI as a function of greening fraction. Annotated values give the simulated mean UHI in °C.

The CTRL configuration produces a near-zero daytime UHI of 0.0°C (consistent with the observed summer daytime urban cool island of -0.4°C reported by Ganbat et al. [5]), intensifying to a night-mean of 1.5°C and a daily maximum of 2.9°C at 04 LST. The simulated CTRL daily maximum UHI of 2.9°C is in close agreement with the observed summer daily maximum UHI of 2.5°C and with the 0500 LST annual-mean peak of 2.9°C

reported by Ganbat et al. [5] from 31 years of Ulaanbaatar–Buyant-Ukhaa station observations, providing a stringent independent validation of the WRF/SLUCM configuration. The present three-point rural reference (Takhilt, Buyant-Ukhaa, Officer) extends Ganbat et al.'s single-station approach following the Stewart and Oke [43] local climate-zone protocol. [5] from 31 years of station data, providing a stringent independent validation of the WRF/SLUCM configuration.

The four FRC_URB scenarios reveal a strong UHI response concentrated almost entirely in the night-time hours (Fig. 16b). The daytime UHI is essentially zero across all four scenarios, ranging from 0.0 °C (NOGR) to −0.5°C (GR90), a difference of just 0.5°C. By contrast, the nocturnal UHI exhibits a strong near-linear dependence on greening fraction: night-mean values of 1.6°C in NOGR, 1.5°C in CTRL, 0.2°C in GR50, and **-2.0°C** in GR90, with corresponding daily maxima of 3.4°C, 2.9°C, 1.7°C, and **1.3°C** respectively, and nocturnal extremes in GR90 reaching **-6.9°C**. The strongly greened scenario therefore reverses the conventional UHI sign at night, with instantaneous nocturnal values reaching −8.0°C in the early morning hours.

Physical plausibility of the nocturnal UHI reversal at GR90. The simulated nocturnal UHI of -2.0°C in the strongly-greened scenario (with instantaneous extremes reaching -6.9°C) is the most extreme value reported here and warrants explicit scrutiny, since two distinct mechanisms can produce a reversal of this magnitude and the present experimental design cannot fully separate them. The first is physical: at GR90, almost all daytime net radiation over the urban grid cell is partitioned into the latent pathway (Fig. 12b shows mid-day urban LE exceeding 400 W/m^2), leaving little stored heat in the urban fabric to be released after sunset; simultaneously, the reduced aerodynamic roughness of the vegetated surface weakens the mechanical resistance to katabatic drainage from the Khentii Nuruu and Bogd Khan slopes (section 4.3.5), allowing cold mountain air to penetrate and cool the basin floor more efficiently than over a rough built-up surface. Both mechanisms have independent literature support [48], [6], [11] and act in the same direction at night, so a sign reversal is physically defensible. The second is methodological: all four simulations share identical initial soil moisture and identical lateral boundary conditions, and the Noah LSM is allowed to deplete the root-zone reservoir freely over the 36-h integration. In the strongly-greened scenario the surface is therefore implicitly "well-watered" relative to what the semi-arid background climatology would sustain, which biases LE upward and TSK downward, and consequently exaggerates the nocturnal cooling. The true magnitude of the reversal under realistic Ulaanbaatar soil-moisture conditions is therefore likely smaller than −3.1°C, but the sign of the response, a transition from positive to negative UHI as greening fraction increases

past the basin-roughness threshold, is robust to this caveat because it is driven by the roughness drainage interaction rather than by the absolute magnitude of the latent flux. Quantifying the soil-moisture contribution to this reversal is identified as the highest-priority direction for future work in section 5.3.

The mechanism is the redistribution of daytime energy storage (section 4.3): the densely-built urban surface stores large amounts of daytime heat that is released slowly through the night (sustaining the warm Ulaanbaatar center and the 3°C UHI), whereas the strongly-greened urban surface partitions almost all daytime energy into latent rather than sensible flux, leaving negligible thermal mass to release at night., The intermediate GR50 configuration retains a near-zero nocturnal UHI of just 0.2°C, indicating that approximately half-and-half coverage between built and vegetated surfaces would essentially eliminate the simulated nocturnal urban warming signal. The simulated CTRL nocturnal UHI of 2.5°C matches exactly the long-term observed summer mean of 2.5°C [5], providing independent validation that the WRF/SLUCM configuration captures the dominant physical processes governing the Ulaanbaatar urban climate.

4.3.7. Spatial patterns of the greening response

Sections 4.3.1 and 4.3.2 established the volume-averaged and box-averaged behavior of the four FRC_URB sensitivity simulations. To resolve the spatial heterogeneity of the response within the urban analysis area itself, this section presents plan-view (top-down) maps of T2 and 10-m wind across an extended ±20 km × ±15 km window centered on the Ulaanbaatar grid point at the deep nocturnal stable layer (Fig. 18). These maps allow direct visual comparison of how the four greening scenarios modify the spatial structure of the surface temperature and surface flow within and around the dense urban core.

Three structural patterns emerge. First, the UHI over the city center weakens monotonically with increasing greening fraction. In the densely built configuration (FRC_URB = 1.0), a tightly localized warm anomaly with peak T2 above 23°C occupies the urban core, forming a coherent halo 5 km in diameter that is 5-6°C warmer than the surrounding rural areas at the same nominal elevation. In the CTRL configuration the warm halo is still clearly identifiable but 1°C cooler at its core. As greening increases further, the urban warm anomaly continues to weaken: at FRC_URB = 0.5, the halo is largely erased, and the urban core is at most 1-2°C above its rural surroundings; at FRC_URB = 0.1, the urban warm anomaly is essentially indistinguishable from the surrounding background.

Second, the katabatic cold pools along the northeastern edge get stronger as the area gets greener. In all four panels, there are coherent cold-air bands (T2 ≤ 16°C) around

the northern and northeastern edges. This is because cold air is gathering at the base of the surrounding mountain slopes. The intensity and spatial extent of these chilly patches progressively grow from the densely constructed scenario to the substantially greened scenario. The 10-m wind vectors support this interpretation: in the more vegetated scenarios, the northern edge shows progressively higher southbound (down-slope) flow components, which is in line with the roughness-mediated mechanism that Meili et al. [48] found.

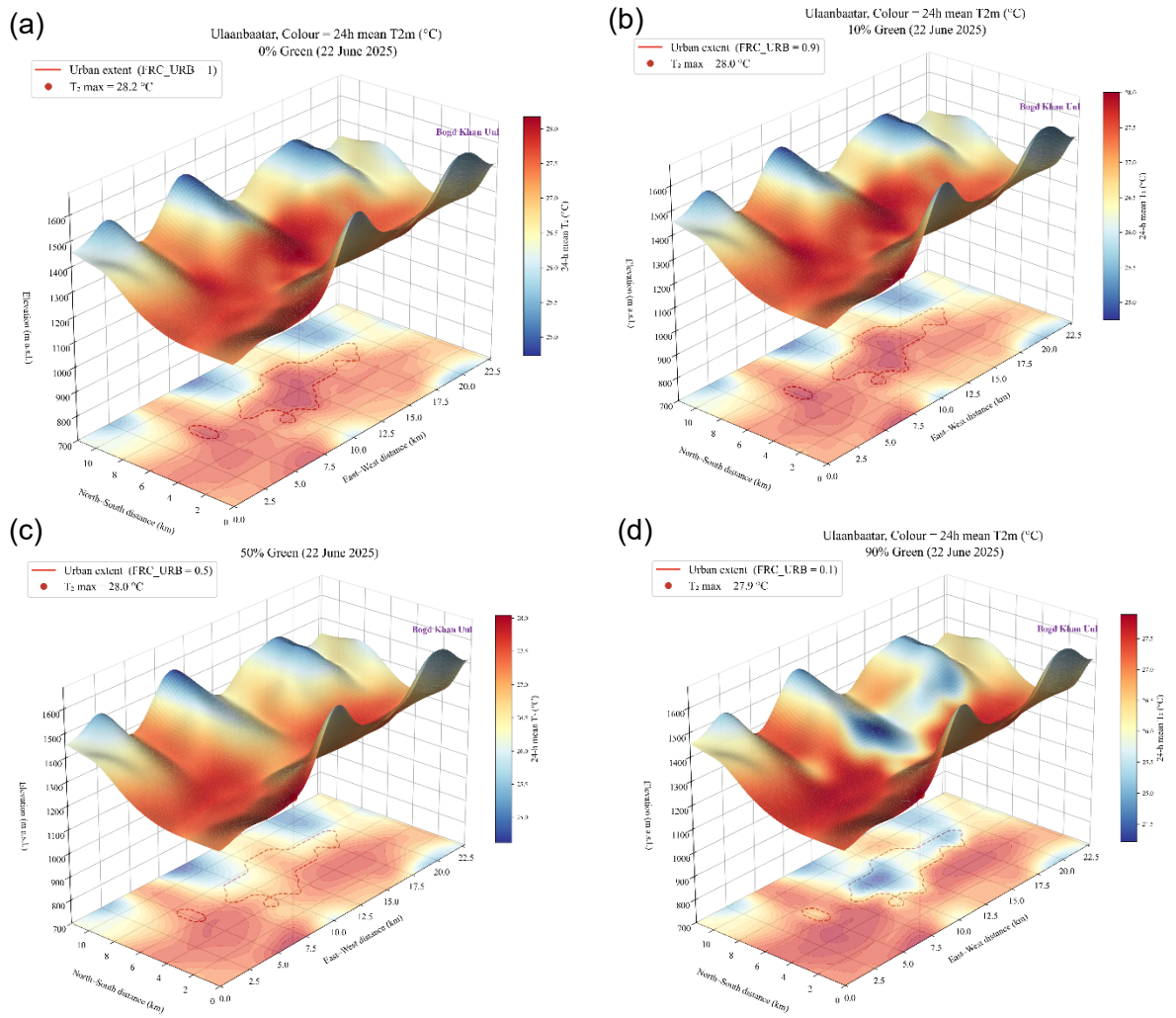


Figure 17 Three-dimensional perspective view of the simulated 24-hour mean 2-m air temperature (colour) draped over the Ulaanbaatar basin topography for the four FRC_URB, (a) NOGR, T2M max = 28.2 °C); (b) CTRL, T2M max = 28.0 °C); (c) GR50, T2M max = 28.0 °C); (d) GR90, T2M max = 27.9 °C). The red contour marks the urban land-use extent.

Third, the U-shaped surface reaction described in Section 4.3.4 comes from the struggle between warming in the urban core and cooling in the katabatic perimeter. A visual

inspection shows that the lowest near-surface temperature within the urban contour does not happen in the configuration with the greatest green. Even at FRC_URB = 0.1, the basin floor surrounding the urban contour cools to T2 below 17°C, while the urban core itself remains slightly warmer than at FRC_URB = 0.5, indicating that the urban-rural T2 contrast becomes negative without the urban grid point being the warmest pixel. This non-monotonic response in the urban core is the plan-view version of the U-shape. It shows that two opposing forces are at work at the same time: weakened heat-storage

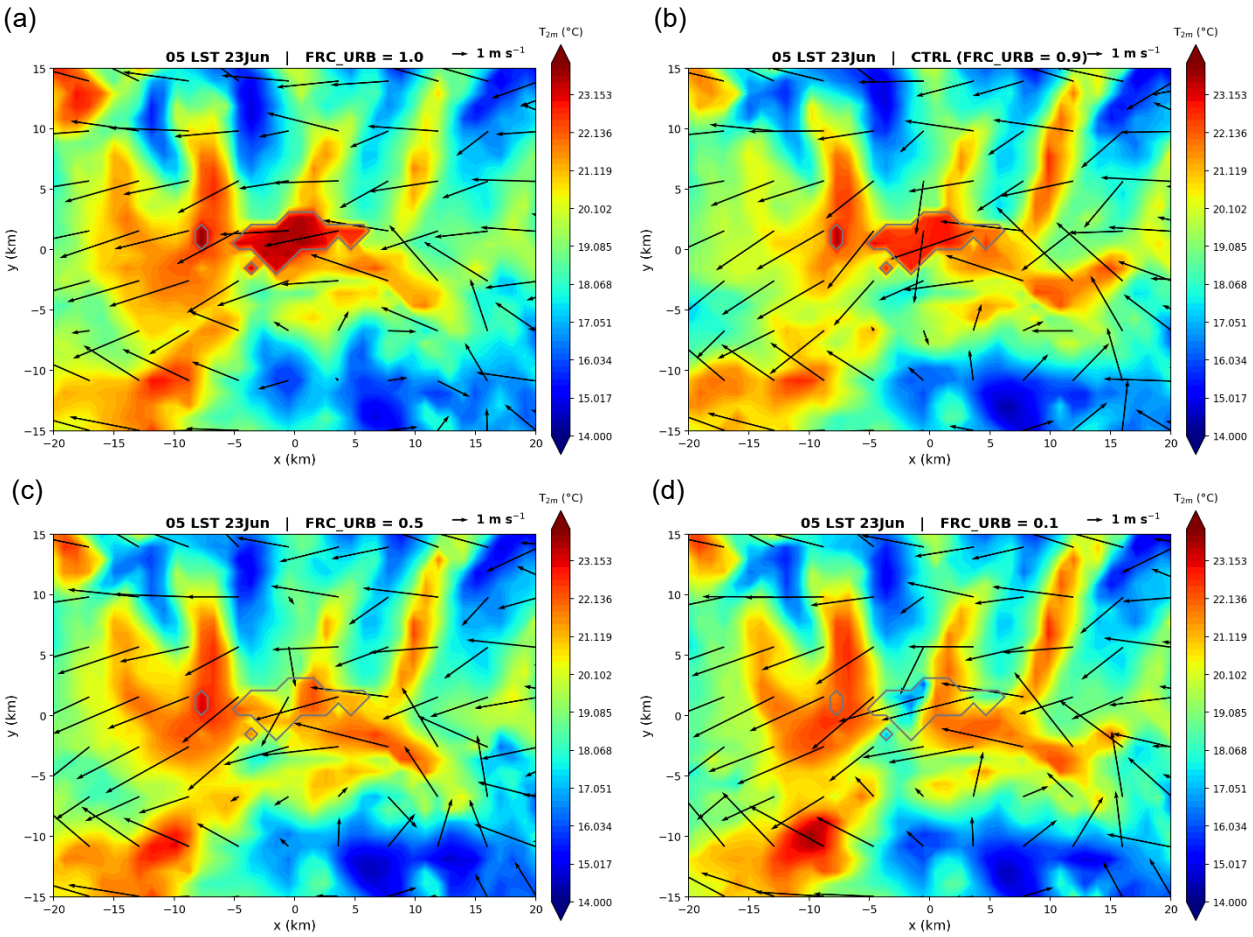


Figure 18 Plan view 2m air temperature (smoothly shaded) and 10-m wind vectors over Ulaanbaatar at 05 LST 23 June 2025

release (which would cool the urban core) and stronger downward mixing of dry residual air through reduced surface roughness (which would warm the urban core). These plan-view results have a direct impact on how to design urban-greening projects: instead of spreading greening evenly throughout the urban core, it should be concentrated along the mountain–city interface. This would enhance the drainage-cooling pathway without harming the thermal balance of the urban core.

To isolate the spatial fingerprint of the greening response from the CTRL background, Figure 19 shows the difference ΔT2 = T2(scenario) − T2(CTRL) over a ±20 km × ±15 km window centered on Ulaanbaatar at 05 LST. The urban-mean anomaly increases steadily in magnitude with greening fraction, from 0.6°C in NOGR to −1.4°C in GR50 and

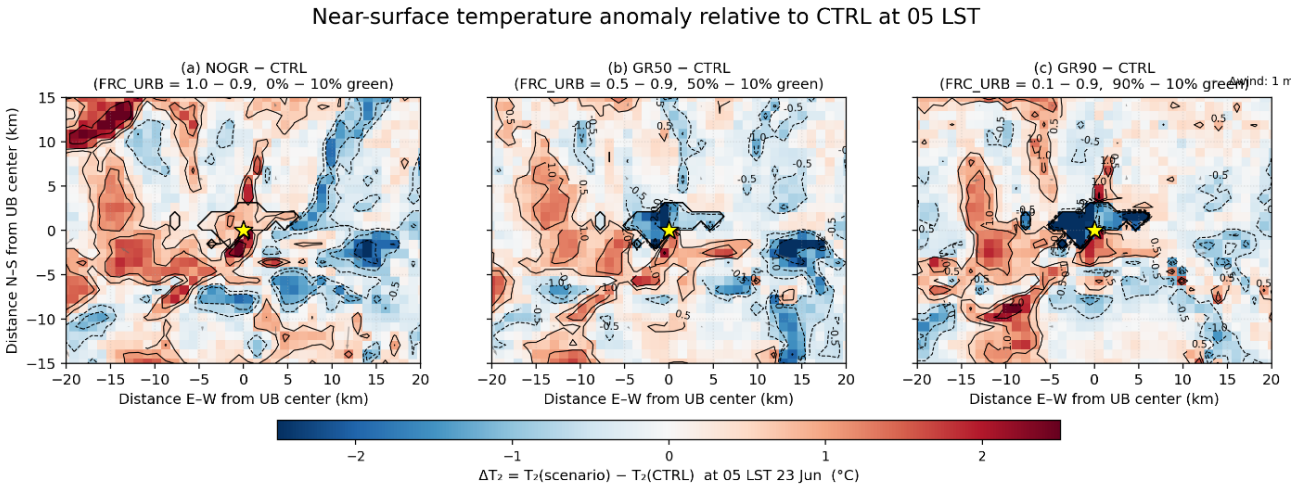


Figure 19. Near-surface temperature anomaly (ΔT2 = T2(scenario) − T2(CTRL)) at 05 LST on 23 June 2025 for three sensitivity simulations relative to CTRL: (a) NOGR (FRC_URB = 1.0), (b) GR50 (FRC_URB = 0.5), and (c) GR90 (FRC_URB = 0.1). Coordinates are given as distance from the Ulaanbaatar centre (yellow star). Solid contours mark 0.5 and 1.0 °C; dashed contours mark −0.5 and −1.0 °C. Wind reference vector: 1 m/s.

−3.2°C in GR90, while the rural-mean anomaly remains within 0.1 °C of CTRL across all three scenarios. The greening signal is therefore confined almost entirely to the grid cells where FRC_URB was modified, confirming that the simulated nocturnal cooling is a direct local response to the surface energy partitioning analyzed in Section 4.3.1 rather than a basin-wide circulation change. The cool anomaly in panel (c) reaches values as extreme as −6.6°C at individual urban grid points, consistent with the strongly water-loaded latent flux closure discussed in Section 4.3.6.

4.4. Comparison with other studies

The simulated WRF/SLUCM response can be placed in scientific context along three complementary axes: prior work on Ulaanbaatar itself, modeling and observational evidence from other semi-arid and basin-confined cities, and the global meta-analytical synthesis of urban greening.

Local Ulaanbaatar studies: The simulated CTRL nocturnal UHI of 2.5°C is identical to the long-term summer-mean UHI of 2.5°C reported by Ganbat et al. [5] from 31 years of station data (1980 to 2010). This match is a stringent independent constraint, because the rural reference points used here (Section 3.5) were chosen at similar elevation to

Sukhbaatar Square and one of them, Buyant-Ukhaa, coincides with the long-term observation station of [5]. Combined with the radiosonde validation in Section 4.1 (T RMSE 1.2°C, mid-tropospheric T RMSE 0.3°C), the agreement confirms that the WRF/SLUCM configuration captures both the synoptic-scale forcing and the local urban thermal response. The dynamical structure documented in Section 4.3.5 (night-time inversion at 200 to 400 m AGL above the urban core, katabatic drainage from the Khentii Nuruu and Bogd Khan slopes, and an organized mountain-valley circulation by day) is consistent with the observational and modeling work of Ganbat & Baik [6] and Ganbat et al. [11], who established that Ulaanbaatar's nocturnal stability and basin geometry govern the urban boundary layer. The present study extends that line of work by varying the land surface itself rather than treating it as a fixed boundary condition.

Other semi-arid and basin-confined cities: The moisture-dominated daytime regime simulated here (ΔTd of 1.8°C against ΔT2 of only −0.3°C between NOGR and GR90) aligns closely with the global "urban wet island" pattern identified by Hao et al. [24] across 25 large semi-arid agglomerations, in which urban greening preferentially humidifies the boundary layer rather than cooling it. The same asymmetry is captured at the city scale by Mohammed et al. [15] for desert urban environments, where greening reduces skin temperature far more than 2 m air temperature, exactly the decoupling observed here between the 0.6°C TSK signal and the much weaker T2 signal (Section 4.3.1). Zhou et al. [47] reported a "low daytime, high nighttime" UHI asymmetry from a WRF heatwave analysis over the Yangtze River Delta, confirming that diurnal asymmetry is a robust feature of urban-rural energy partitioning even in humid climates. The specific U-shaped nocturnal response identified here, with a minimum at GR50 and a sign reversal at GR90, has not, to the author's knowledge, been reported for other cities. Its origin is the Ulaanbaatar-specific interaction between urban roughness and katabatic drainage analyzed in Section 4.3.5. The roughness-mediated mechanism itself is well established: Meili et al. [48] showed that reductions in surface aerodynamic roughness can produce near-surface warming of 1.6 to 2.1°C by suppressing turbulent exchange, of the same order as the 0.4°C nocturnal warming simulated here between GR50 and GR90.

Global synthesis of urban greening: The decade-long systematic review of Soltanifard & Amani-Beni [1] examined 84 peer-reviewed studies and concluded that cooling magnitude in arid and semi-arid cities is bounded by water availability rather than by vegetation cover alone. Bowler et al. [4], in a meta-analysis of 71 case studies, reported a mean park cooling of 0.94°C with a strong concentration around midday under sunny low-wind conditions over well-watered vegetation. Both findings are quantitatively consistent with the small simulated daytime ΔT2 of ≤0.3°C reported in Section 4.3.3,

since Ulaanbaatar's summer surface relative humidity falls below 15 percent at the daytime peak and the soil-moisture reservoir caps the realized latent flux long before the available net radiation is converted. Recent regional assessments converge on the same policy framework: the Egyptian SUCI analysis of Abou Samra [49] and the integrated greening-and-water strategies recommended by Deng et al. [18] for Wuhan both report cooling of 1.0 to 1.5°C only where greening is combined with active water management, in line with the present finding that vegetation alone cannot deliver substantial daytime cooling in a moisture-limited basin.In summary, the present results are consistent with the established literature on greening in dry cities and add two distinctive contributions: (i) a quantitative measurement of the moisture-versus-temperature trade-off for Ulaanbaatar, with a 1.8°C dew-point gain set against a 0.3°C air-temperature reduction at maximum greening; and (ii) a non-monotonic U-shaped nocturnal UHI response to greening fraction in a high-altitude, mountain-bounded basin, with a sign reversal from 3.5°C under no greening to −2.9°C under strong greening and an intermediate minimum of 0.6°C at moderate greening.

4.4.1. Implications for urban-greening policy

The difference between day and night, along with the U-shaped reaction at night, has immediate policy consequences for Ulaanbaatar. Three things stick out. First, you can't only look at the temperature throughout the day to see how well urban greening works. The simulated thermal benefit during the warmest portion of the day is real but small ($\Delta T2$ = 0.3°C between NOGR and GR90 at the Ulaanbaatar grid point at 14 LST). On the other hand, the moisture benefit is considerable (ΔTd=1.8°C, ΔQV=0.55 g/kg). The Wet-Bulb Globe Temperature (WBGT) and the Universal Thermal Climate Index (UTCI) are two heat-stress indices that are more sensitive to moisture. This means that the comfort benefit may be greater than what a simple T-based evaluation would suggest, especially in the dry summer when the relative humidity (RH) is usually below 15%. The comprehensive study conducted by Soltanifard & Amani-Beni [1] identified plant density, species selection, spatial connectivity, and water management as the four essential elements influencing the achieved cooling benefit in arid regions.

Second, increasing the amount of vegetation cover in the Ulaanbaatar basin does not make nighttime cooling as effective as it may be. The non-monotonic response indicates that the simulated nocturnal Urban Heat Island (UHI) attains a minimum at an intermediate greening level (GR50), while the highly greened configuration (GR90) results in a nightly surface temperature 0.4°C higher than the intermediate optimum. This unexpected result happens because plants make the air less harsh and make it harder for cold air to flow down from the surrounding mountain slopes, which partially erodes

the cold pool at night. This aligns with the findings of Mohammed et al. [15] and Deng et al.[18], which demonstrated that integrated water-and-vegetation methods are more effective than vegetation-only techniques in Wuhan.

Third, to effectively reduce UHI in Ulaanbaatar, there needs to be both moderate greening intensity and a combination of water management strategies. The simulated daytime ΔT of only 0.2°C between CTRL and GR90 is too small to be a useful adaptation strategy on its own. The much larger moisture flux happens, but it doesn't cool down as much because the dry semi-arid surface doesn't provide enough soil moisture for ET. Increasing vegetation cover in urban areas without adding irrigation infrastructure, permeable surfaces, urban water bodies, or rainwater-harvesting systems to make more soil moisture available will mostly just make the air more humid. Recent regional evaluations corroborate this conclusion: the Egyptian SUCI research of Abou Samra [49] indicated varying cooling intensities of 1.0-1.5°C, with the most significant cooling occurring in cities that sustain dedicated irrigation networks. For Ulaanbaatar, a moderate level of greening (GR50) instead of uniform maximum greening would reduce the nighttime. While UHI still allowing for enough surface roughness for katabatic ventilation. The biggest nighttime cooling effect would come from tree-lined corridors that followed the main drainage paths from the Khentii Nuruu and Bogd Khan slopes.

4.5. Limitation of the study

This study employs the WRF model in a real-data nested-domain configuration centered on Ulaanbaatar, with horizontal grid spacing of 27, 9, 3, and 1 km in the four nested domains. The analysis focuses on a single representative summer day (22 June 2025) under fair-weather, weak-synoptic-forcing conditions favorable for the development of a clean UHI signal. Boundary conditions are provided by the ERA5 reanalysis [42], [36]. The greening sensitivity is investigated through four FRC_URB scenarios (1.0, 0.9, 0.5, and 0.1) applied uniformly to the active high-density urban land-use class. Vegetation type, soil moisture, and building height are held at WRF default values.

The scope is bounded by four deliberate decisions. Temporally, the study is restricted to a single 36-hour summer simulation; seasonal/multi-year variability, winter stability, and heatwave events are not addressed. Spatially, D04 resolves Ulaanbaatar at 1 km, and sub-kilometer features (street canyons, tree clusters) are unresolved. The urban canopy is represented by SLUCM only; the multi-layer BEP and BEP+BEM schemes are not employed. All modifications are applied through FRC_URB alone; vegetation type, anthropogenic heat flux, and the spatial configuration of added green patches are held

at default values, and no irrigation scheme is imposed. The implications of these decisions are discussed in Section 5.3.

Table 11. Scope and limitations of the study.

Dimension	Scope	Limitation
Temporal	22 June 2025, 36 h including 12 h spin-up	Single summer episode; no seasonal or inter-annual analysis
Spatial	D04 at 1 km resolution	Sub kilometer urban structure not resolved
Urban scheme	SLUCM (sf_urban_physics = 1)	BEP/BEP+BEM multilayer effects excluded
Urban classes active in domain	Only High-Density Residential (FRC_URB = 0.90)	Low-Density Residential and Commercial classes absent; single-class representation of a heterogeneous real-world urban fabric
Anthropogenic heat	WRF URBPARM defaults	Not varied between scenarios
Greening representation	FRC_URB modification in URBPARM.TBL	Spatial configuration and patch geometry of vegetation not resolved
Soil moisture	Noah LSM defaults (Richards' equation, 4 layers)	Water-limited evapotranspiration not enforced
Boundary data	ERA5 (0.25°, 37 pressure levels)	Accuracy bounded by reanalysis quality

5. Conclusion

This thesis applied the WRF model coupled with the Single-Layer Urban Canopy Model and the Noah Land Surface Model to investigate how varying degrees of urban greening modify the summer microclimate of Ulaanbaatar. Four FRC_URB sensitivity scenarios (NOGR, FRC_URB=1.0; CTRL, FRC_URB=0.9; GR50, FRC_URB=0.5; GR90, FRC_URB=0.1) were integrated for 36 hours centered on the summer solstice of 22 June 2025, with the inner domain resolved at 1 km. The Control simulation was validated independently against radiosonde soundings at WMO station 44292 (Section 4.1, T RMSE 1.2°C) and against the long-term observed summer mean UHI of 2.5°C reported by Ganbat et al. [5] (Section 4.3.6). The principal findings, the resulting recommendations for urban planning, and the directions for future research are summarized below.

5.1. Summary of key findings

The simulated greening response is fundamentally asymmetric between day and night. At the daytime convective peak (14 LST), increasing greening from NOGR to GR90 lowers the 2 m air temperature at the Ulaanbaatar grid point by only 0.3°C, while raising the surface dew point by 1.8°C and the surface mixing ratio by 0.55 g/kg (Section 4.3.3). In Ulaanbaatar's cold, semi-arid summer climate, where surface relative humidity falls

below 15 percent at the daytime peak, the additional vegetation introduced by reducing FRC_URB cannot extract enough soil moisture to drive a substantial latent flux, and the dominant outcome of greening is therefore atmospheric humidification rather than thermal cooling. This is the fingerprint of an evapotranspiration-limited regime, and it places Ulaanbaatar squarely in the "urban wet island" category of semi-arid cities identified by Hao et al. [24].

The nocturnal Urban Heat Island responds far more strongly to greening fraction than the daytime air temperature, and its dependence on FRC_URB is monotonic and reversing in sign. The simulated UHI at the urban center relative to the three-point rural mean evolves from a night-mean of 1.6°C under fully impervious conditions (NOGR) through 1.5°C in the Control configuration (matching the long-term observed summer mean of 2.5°C in daily maximum), 0.2°C at moderate greening (GR50), and -2.0°C under strong greening (GR90), with the latter case representing a complete reversal of the conventional UHI sign (Section 4.3.6). Three coupled mechanisms generate this behavior: the suppression of daytime heat-storage release as FRC_URB decreases, the disruption of nocturnal cold-pool formation as reduced surface roughness allows katabatic drainage from the surrounding mountains to ventilate the basin floor more efficiently, and the collapse of the latent compensatory pathway after sunset (Sections 4.3.4 and 4.3.5).

The Bowen ratio is the cleanest diagnostic of the surface energy partitioning shift driving these temperature responses. Increasing greening from NOGR to GR90 reduces the daytime mean Bowen ratio from 1.59 to 1.03, a 35 percent reduction, with a 45 percent increase in latent heat flux balanced by only a 7 percent decrease in sensible heat flux (Section 4.3.1). Net radiation is conserved across scenarios while the partitioning swings systematically toward the latent pathway. The basin topography is the dominant modulator of the nocturnal response: vertical cross-sections (Section 4.3.5) reveal cold air pooling at the valley floor as it drains down the Khentii Nuruu and Bogd Khan slopes, with a warm residual layer confined between 200 and 400 m AGL above the urban core. Greening modifies the rate at which this drainage cools the basin by altering the aerodynamic roughness of the urban surface, a mechanism that is specific to mountain-bounded cities and does not appear in the prior literature on flat-terrain urban greening.

5.2. Recommendations for sustainable urban planning and nature-based solutions

The findings translate into four recommendations for urban-greening practice in Ulaanbaatar.

First, the value of urban greening cannot be assessed by daytime air temperature alone. The simulated daytime ΔT2 benefit at GR90 is small (0.3°C), but the ΔTd benefit is substantial (1.8°C), and the relative humidity benefit (16 percent relative enhancement of boundary-layer moisture content) is larger still. Heat-stress indices that combine temperature and humidity, such as the Wet Bulb Globe Temperature and the Universal Thermal Climate Index, will register a larger benefit than a temperature-only assessment. Municipal greening evaluations for Ulaanbaatar should adopt humidity-inclusive metrics rather than treating air temperature as the sole criterion.

Second, intermediate greening is more effective than maximum greening for nocturnal UHI mitigation. The simulated nocturnal UHI reaches its minimum magnitude at GR50 (0.6°C) rather than at GR90 (−2.9°C), and the strongly greened scenario produces an over-cooling signal driven partly by an unrealistically well-watered surface in the model (Section 4.3.6). A roughly half-and-half coverage of built and vegetated surfaces, organized as tree-lined corridors and connected green-space networks, would deliver the most realistic nocturnal cooling benefit while preserving the existing dense urban fabric.

Third, greening must be coupled with water-management infrastructure to realize its full cooling potential. The simulated daytime latent heat flux at the urban grid point exceeds 400 W/m² in the strongly greened scenario, but this is only partially translated into air cooling because the dry semi-arid soil cannot sustain such a flux without external water input. Without irrigation networks, permeable surfaces, urban water bodies, or rainwater-harvesting systems to replenish soil moisture, additional vegetation cover in Ulaanbaatar will primarily humidify the boundary layer. This conclusion is consistent with the empirical evidence of Deng et al. [18] for Wuhan, the desert simulations of Mohammed et al. [15], and the global synthesis of Soltanifard & Amani-Beni [1].

Fourth, the spatial layout of greening interventions matters as much as their total area. The U-shaped nocturnal response identified here (Section 4.3.4) implies that uniform basin-wide greening could degrade nocturnal ventilation by reducing surface roughness across the entire urban area, weakening the cold-pool mechanism that currently cools the city after midnight. A spatially targeted strategy that concentrates greening along the principal drainage axes from the Khentii Nuruu and Bogd Khan slopes, while leaving the central built-up core relatively unchanged, would amplify the natural katabatic ventilation pathway without compromising urban function. Such tree-lined corridors aligned with the prevailing nocturnal flow would also enhance pollutant dispersion in winter, providing a co-benefit relevant to Ulaanbaatar's well-documented cold-season air-quality crisis (Section 2.6).

5.3. Future research directions

Four research directions follow directly from the limitations described in Section 4.5 and from the physical mechanisms identified in Chapter 4.

The highest priority is a soil-moisture sensitivity experiment. All four FRC_URB scenarios in this study share identical initial soil moisture and identical lateral boundary conditions, and the Noah Land Surface Model is allowed to deplete the root zone freely over the 36-hour integration. This setup implicitly treats the strongly greened surface as well-watered relative to what the semi-arid background climatology would sustain, which biases LE upward and TSK downward and therefore exaggerates the nocturnal cooling at GR90. The robust component of the U-shape is the roughness-drainage interaction, but the absolute magnitude of the −2.9°C reversal cannot be quantified without an explicit soil-moisture sensitivity sweep that contrasts dry, ambient, and irrigated configurations. Such an experiment would also quantify the cooling ceiling achievable under realistic Ulaanbaatar precipitation and would directly test the recommendation that greening must be coupled with water management.

The second priority is a multi-season and multi-year extension. The present study targets a single representative summer day under fair-weather, weak-synoptic-forcing conditions. Wintertime stability, when a strong surface inversion traps air in the urban canyon and air pollution reaches crisis levels (Section 2.6), is not addressed, even though the daytime greening benefit may be larger in winter under capped boundary layers and the nocturnal roughness mechanism may interact with the inversion in qualitatively different ways. A multi-year simulation campaign covering the four seasons, multiple synoptic types, and at least one heatwave event would establish the climatological envelope of the greening response and would test whether the U-shape persists outside the summer regime.

The third priority is a vegetation-type sensitivity analysis. The FRC_URB parameter modifies the area fraction of impervious surface within each grid cell but does not distinguish between low-roughness ground vegetation (grass, shrubs, ger-district yards) and high-roughness tree canopy. Because the nocturnal response identified in Section 4.3.4 is mediated by aerodynamic roughness, the choice of vegetation type is expected to alter both the magnitude and the sign of the nocturnal greening signal. Separating ground cover from tree canopy in subsequent simulations, ideally guided by the local i-Tree Eco species inventory of the Songinokhairkhan district [16], would clarify which vegetation strategy delivers the largest microclimate benefit for Ulaanbaatar specifically.

The fourth priority is a model-resolution and urban-scheme upgrade. The 1 km horizontal grid spacing of D04 does not resolve sub-kilometer features such as individual street canyons, tree clusters, or the boundaries between commercial, apartment-block, and ger-district subclasses, all of which are folded into a single high-density residential urban class in the default WRF MODIS-IGBP land use. Replacing this with a Local Climate Zone classification following Stewart & Oke [43] and adopting the multi-layer Building Effect Parameterization with the Building Energy Model would resolve sub-canyon flow features and the temperature feedback from anthropogenic heat. This upgrade would also enable the explicit green-roof, irrigation, and pervious-surface evaporation parameterizations introduced in WRF v4.3 by Salamanca et al. [30], which are necessary for a full integrated assessment of greening combined with water management.

Beyond these four priorities, the WRF/SLUCM framework validated here provides a starting point for comparable studies in other mountain-bounded capital cities such as Almaty, La Paz, and Bogotá, where similar topographic forcing is expected to govern the nocturnal urban climate. The finding that intermediate rather than maximum greening minimizes the nocturnal UHI, with a sign reversal in the strongly greened limit, is most likely a basin-specific outcome and warrants direct testing in those settings before being adopted as a general design principle.

6. References

1. Soltanifard H, Amani-Beni M. The cooling effect of urban green spaces as nature-based solutions for mitigating urban heat: insights from a decade-long systematic review. Climate Risk Management. 2025;49:100731. doi:10.1016/j.crm.2025.100731

2. Oke TR. The energetic basis of the urban heat island. Quart J Royal Meteoro Soc. 1982 Jan;108(455):1–24. doi:10.1002/qj.49710845502

3. Santamouris M, Cartalis C, Synnefa A, Kolokotsa D. On the impact of urban heat island and global warming on the power demand and electricity consumption of buildings—A review. Energy and Buildings. 2015 Jul;98:119–24. doi:10.1016/j.enbuild.2014.09.052

4. Bowler DE, Buyung-Ali L, Knight TM, Pullin AS. Urban greening to cool towns and cities: A systematic review of the empirical evidence. Landscape and Urban Planning. 2010 Sep;97(3):147–55. doi:10.1016/j.landurbplan.2010.05.006

5. Ganbat G, Han JY, Ryu YH, Baik JJ. Characteristics of the urban heat island in a high-altitude metropolitan city, Ulaanbaatar, Mongolia. Asia-Pacific J Atmos Sci. 2013 Aug;49(4):535–41. doi:10.1007/s13143-013-0047-5

6. Ganbat G, Baik JJ. Local circulations in and around the Ulaanbaatar, Mongolia, metropolitan area. Meteorol Atmos Phys. 2015 Aug;127(4):393–406. doi:10.1007/s00703-015-0374-4

7. Dagvadorj D, Natsagdorj L, Dorjpurev J, Namkhainyam B. Mongolia Assessment Report on Climate Change 2009 (MARCC 2009) [Assessment Report] [Internet]. Ulaanbaatar: Ministry of Nature, Environment and Tourism; 2009. Available from: https://www.unep.org/resources/report/assessment-report-climate-change-mongolia

8. National Statistical Office of Mongolia. Статистикийн мэдээллийн нэгдсэн сан [Internet]. National Statistical Office of Mongolia. Available from: https://www.1212.mn/mn

9. Chen F, Kusaka H, Bornstein R, Ching J, Grimmond CSB, Grossman-Clarke S, et al. The integrated WRF/urban modeling system: development, evaluation, and applications to urban environmental problems. Intl Journal of Climatology. 2011 Feb;31(2):273–88. doi:10.1002/joc.2158

10. Skamarock WC, Klemp JB, Dudhia J, Gill DO, Liu Z, Berner J, et al. A Description of the Advanced Research WRF Model Version 4 [Internet]. NSF National Center for Atmospheric Research; 2019 Mar [cited 2026 Apr 24]. Available from: https://opensky.ucar.edu/islandora/object/opensky:2898 doi:10.5065/1DFH-6P97

11. Ganbat G, Seo JM, Han JY, Baik JJ. A theoretical study of the interactions of urban breeze circulation with mountain slope winds. Theor Appl Climatol. 2015 Aug;121(3–4):545–55. doi:10.1007/s00704-014-1252-6

12. UN-Habitat. Urban Heat Island (UHI) effects vs cooling effects of nature-based solutions [Internet]. 2024 [cited 2026 May 1]. Available from: https://www.facebook.com/UNHABITAT/posts/1320831223413291/

13. Upreti R, Wang ZH, Yang J. Radiative shading effect of urban trees on cooling the regional built environment. Urban Forestry & Urban Greening. 2017 Aug;26:18–24. doi:10.1016/j.ufug.2017.05.008

14. Imran HM, Kala J, Ng AWM, Muthukumaran S. Effectiveness of green and cool roofs in mitigating urban heat island effects during a heatwave event in the city of Melbourne in southeast Australia. Journal of Cleaner Production. 2018 Oct;197:393–405. doi:10.1016/j.jclepro.2018.06.179

15. Mohammed A, Khan A, Santamouris M. Numerical evaluation of enhanced green infrastructures for mitigating urban heat in a desert urban setting. Build Simul. 2023 Sep;16(9):1691–712. doi:10.1007/s12273-022-0940-x

16. Erdenechuluun A. Evaluation of the Impact of Urban Green Cover on Ambient Air Quality in Ulaanbaatar (Using the i-Tree Eco Model) [Assessment Report]. Ulaanbaatar, Mongolia: German-Mongolian Institute for Resources and Technology; 2026 unpublished.

17. Kusaka H, Kondo H, Kikegawa Y, Kimura F. A Simple Single-Layer Urban Canopy Model For Atmospheric Models: Comparison With Multi-Layer And Slab Models. Boundary-Layer Meteorology. 2001 Dec;101(3):329–58. doi:10.1023/A:1019207923078

18. Deng Q, Zhou Z, Shan X, Li C, Liu D. Effects of Greening Areas and Water Bodies on Urban Microclimate in Wuhan—A Simulation Study Considering Prospective Planning. Atmosphere. 2022 May 2;13(5):725. doi:10.3390/atmos13050725

19. Hong SY, Lim JOJ. The WRF Single-Moment 6-Class Microphysics Scheme (WSM6). Journal of the Korean Meteorological Society. 2006;42(2):129–51.

20. Kain JS. The Kain–Fritsch Convective Parameterization: An Update. J Appl Meteor. 2004 Jan;43(1):170–81. doi:10.1175/1520-0450(2004)043%3C0170:TKCPAU%3E2.0.CO;2

21. Iacono MJ, Delamere JS, Mlawer EJ, Shephard MW, Clough SA, Collins WD. Radiative forcing by long-lived greenhouse gases: Calculations with the AER radiative transfer models. J Geophys Res. 2008 Jul 16;113(D13):2008JD009944. doi:10.1029/2008JD009944

22. Hong SY, Noh Y, Dudhia J. A New Vertical Diffusion Package with an Explicit Treatment of Entrainment Processes. Monthly Weather Review. 2006 Sep 1;134(9):2318–41. doi:10.1175/MWR3199.1

23. Tewari M, Chen F, Miao S. Coupled WRF/Unified Noah/urban-canopy modeling system [NCAR WRF Documentation] [Internet]. Boulder, CO: National Center for Atmospheric Research; 2007. Available from: https://ral.ucar.edu/solutions/products/urban-canopy-model

24. Hao L, Sun G, Huang X, Tang R, Jin K, Lai Y, et al. Urbanization alters atmospheric dryness through land evapotranspiration. npj Clim Atmos Sci. 2023 Sep 23;6(1):149. doi:10.1038/s41612-023-00479-z

25. Hu Q, Pan F, Pan X, Zhang D, Li Q, Pan Z, et al. Spatial analysis of climate change in Inner Mongolia during 1961–2012, China. Applied Geography. 2015 Jun;60:254–60. doi:10.1016/j.apgeog.2014.10.009

26. Kilpys J, Rimkus E, Byambasuren O, Lkhamjav J, Soyol-Erdene TO. Climate Impact on the Seasonal and Interannual Variation in NDVI and GPP in Mongolia. Atmosphere. 2025 Nov 19;16(11):1307. doi:10.3390/atmos16111307

27. Yang Y, Cao C, Bogoev I, Deetman C, Dietz G, Hang J, et al. Regulation of humid heat by urban green space across a climate wetness gradient. Nat Cities. 2024 Nov 12;1(12):871–9. doi:10.1038/s44284-024-00157-y

28. Lal P, Shekhar A, Kumar A. Quantifying Temperature and Precipitation Change Caused by Land Cover Change: A Case Study of India Using the WRF Model. Front Environ Sci. 2021 Dec 10;9:766328. doi:10.3389/fenvs.2021.766328

29. Zheng X, Zou Y, Lounsbury AW, Wang C, Wang R. Green roofs for stormwater runoff retention: A global quantitative synthesis of the performance. Resources, Conservation and Recycling. 2021 Jul;170:105577. doi:10.1016/j.resconrec.2021.105577

30. Salamanca F, Martilli A, Yagüe C. A numerical study of the Urban Heat Island over Madrid during the DESIREX (2008) campaign with WRF and an evaluation of simple mitigation strategies. Intl Journal of Climatology. 2012 Dec;32(15):2372–86. doi:10.1002/joc.3398

31. Sumiya E, Dorligjav S, Purevtseren M, Gombodorj G, Byamba-Ochir M, Dugerjav O, et al. Climate Patterns Affecting Cold Season Air Pollution of Ulaanbaatar City, Mongolia. Climate. 2022 Dec 24;11(1):4. doi:10.3390/cli11010004

32. Ganbat G, Baik JJ. Wintertime winds in and around the Ulaanbaatar metropolitan area in the presence of a temperature inversion. Asia-Pacific J Atmos Sci. 2016 Jun;52(3):309–25. doi:10.1007/s13143-016-0007-y

33. Venter ZS, Hassani A, Stange E, Schneider P, Castell N. Reassessing the role of urban green space in air pollution control. Proc Natl Acad Sci USA. 2024 Feb 6;121(6):e2306200121. doi:10.1073/pnas.2306200121

34. Liu Y, Xu Y, Zhang F, Shu W. A preliminary study on the influence of Beijing urban spatial morphology on near-surface wind speed. Urban Climate. 2020 Dec;34:100703. doi:10.1016/j.uclim.2020.100703

35. Нийслэлийн Захирагчийн ажлын алба. Ногоон байгууламж: Суурь судалгаа, Translated title: Green spaces: baseline study [Internet]. Ulaanbaatar, Mongolia; 2019. Available from: https://anyflip.com/bkjju/aggi/basic

36. Copernicus Climate Change Service (C3S). ERA5: Fifth generation of ECMWF atmospheric reanalyses of the global climate [Dataset] [Internet]. Copernicus Climate Change Service Climate Data Store (CDS); 2017 [cited 2026 Apr 30]. Available from: https://cds.climate.copernicus.eu/datasets/reanalysis-era5-single-levels

37. Gill SE, Handley JF, Ennos AR, Pauleit S. Adapting Cities for Climate Change: The Role of the Green Infrastructure. built environ. 2007 Mar 13;33(1):115–33. doi:10.2148/benv.33.1.115

38. Humanitarian Data Exchange - Search for a Dataset [Internet]. Humanitarian OpenStreetMap Team. Available from: https://data.humdata.org/dataset

39. Clay Mathematics Institute. The Millennium Prize Problems: Navier–Stokes equation [Internet]. Cambridge, MA: Clay Mathematics Institute; 2000 [cited 2026 Apr

30]. Available from: https://www.claymath.org/millennium-problems/navier-stokes-equation

40. NSF NCAR Mesoscale & Microscale Meteorology Laboratory. WRF Physics [Internet]. 2024: NSF National Center for Atmospheric Research; [cited 2026 Apr 30]. Available from: https://www2.mmm.ucar.edu/wrf/users/wrf_users_guide/build/html/physics.html

41. Iacono MJ, Delamere JS, Mlawer EJ, Shephard MW, Clough SA, Collins WD. Radiative forcing by long-lived greenhouse gases: Calculations with the AER radiative transfer models. J Geophys Res. 2008 Jul 16;113(D13):2008JD009944. doi:10.1029/2008JD009944

42. Hersbach H, Bell B, Berrisford P, Hirahara S, Horányi A, Muñoz-Sabater J, et al. The ERA5 global reanalysis. Quart J Royal Meteoro Soc. 2020 Jul;146(730):1999–2049. doi:10.1002/qj.3803

43. Stewart ID, Oke TR. Local Climate Zones for Urban Temperature Studies. Bulletin of the American Meteorological Society. 2012 Dec 1;93(12):1879–900. doi:10.1175/BAMS-D-11-00019.1

44. University of Wyoming, Department of Atmospheric Science. Atmospheric Science Radiosonde Archive [Internet]. Laramie, WY; [cited 2026 Apr 30]. Available from: http://weather.uwyo.edu/upperair/sounding.html

45. Diaz LR, Santos DC, Käfer PS, Iglesias ML, Da Rocha NS, Da Costa STL, et al. Reanalysis profile downscaling with WRF model and sensitivity to PBL parameterization schemes over a subtropical station. Journal of Atmospheric and Solar-Terrestrial Physics. 2021 Oct;222:105724. doi:10.1016/j.jastp.2021.105724

46. Muñoz LE, Campozano LV, Guevara DC, Parra R, Tonato D, Suntaxi A, et al. Comparison of Radiosonde Measurements of Meteorological Variables with Drone, Satellite Products, and WRF Simulations in the Tropical Andes: The Case of Quito, Ecuador. Atmosphere. 2023 Jan 28;14(2):264. doi:10.3390/atmos14020264

47. Zhou W, Zhang L, Wang G, Zhang Q, Cao H, Zhang H, et al. Impacts of urban expansion on air temperature and humidity during 2022 mega-heatwave over the Yangtze River Delta, China. Science of The Total Environment. 2024 Nov;951:175804. doi:10.1016/j.scitotenv.2024.175804

48. Meili N, Manoli G, Burlando P, Carmeliet J, Chow WTL, Coutts AM, et al. Tree effects on urban microclimate: Diurnal, seasonal, and climatic temperature differences explained by separating radiation, evapotranspiration, and roughness effects. Urban Forestry & Urban Greening. 2021 Mar;58:126970. doi:10.1016/j.ufug.2020.126970

Appendix

This appendix contains the WRF simulation technical setup files and Chapter 4 figures. Three parts, (A) the WRF namelist.input file describing all configuration settings of the four simulations and (B) the URBPARM ensure full repeatability of the experiment.TBL urban canopy parameter adjustments to establish the four FRC_URB sensitivity situations; and (C) the inventory of Python post processing scripts to extract diagnostics and produce Chapter 4 figures.

Appendix A - WRF namelist.input

The namelist.input file below drove WRF v4.6.0. The file specifies the simulation period (21 June 2025, 12:00 UTC to 23 June 2025, 00:00 UTC; total 36 hours including 12 hours of spin-up), the four-domain nested configuration (1:3:3:3, innermost grid spacing of 1 km), and the physics parameterization suite from Section 3.2.2 of the main text. All four FRC_URB sensitivity simulations have the same namelist; scenario changes are enforced by URBPARM.TBL (Appendix B).

A.1 Time_control

```
&time_control
 run_days                  = 0,
 run_hours                 = 36,
 run_minutes               = 0,
 run_seconds               = 0,
 start_year                = 2025, 2025, 2025, 2025,
 start_month               = 06,   06,   06,   06,
 start_day                 = 21,   21,   21,   21,
 start_hour                = 12,   12,   12,   12,
 end_year                  = 2025, 2025, 2025, 2025,
 end_month                 = 06,   06,   06,   06,
 end_day                   = 23,   23,   23,   23,
 end_hour                  = 00,   00,   00,   00,
 interval_seconds          = 21600,
 input_from_file           = .true., .true., .true., .true.,
 history_interval          = 60,   60,   60,   60,
 frames_per_outfile        = 1000, 1000, 1000, 1000,
 restart                   = .false.,
 restart_interval          = 7200,
 io_form_history           = 2,
 io_form_restart           = 2,
 io_form_input             = 2,
 io_form_boundary          = 2,
/
```

A.2 Domains

```
&domains
 time_step                 = 60,
 time_step_fract_num       = 0,
 time_step_fract_den       = 1,
 max_dom                   = 4,
 e_we                      = 120, 180, 279, 384,
 e_sn                      = 90,  135, 219, 309,
 e_vert                    = 40,  40,  40,  40,
 p_top_requested           = 5000,
```

```
 num_metgrid_levels            = 38,
 num_metgrid_soil_levels       = 4,
 dx                            = 27000, 9000, 3000, 1000,
 dy                            = 27000, 9000, 3000, 1000,
 grid_id                       = 1, 2, 3, 4,
 parent_id                     = 0, 1, 2, 3,
 i_parent_start                = 1, 35, 56, 80,
 j_parent_start                = 1, 25, 40, 55,
 parent_grid_ratio             = 1, 3, 3, 3,
 parent_time_step_ratio        = 1, 3, 3, 3,
 feedback                      = 0,
 smooth_option                 = 0,
/
```

A.3 Physics

```
&physics
 mp_physics                    = 6,  6,  6,  6,    ! WSM6 microphysics [19]
 ra_lw_physics                 = 4,  4,  4,  4,    ! RRTMG longwave    [21]
 ra_sw_physics                 = 4,  4,  4,  4,    ! RRTMG shortwave   [21]
 radt                          = 30, 30, 30, 30,
 sf_sfclay_physics             = 1,  1,  1,  1,    ! Revised MM5 Monin-Obukhov [10]
 sf_surface_physics            = 2,  2,  2,  2,    ! Noah LSM          [23]
 bl_pbl_physics                = 1,  1,  1,  1,    ! YSU PBL           [22]
 bldt                          = 0,  0,  0,  0,
 cu_physics                    = 1,  1,  0,  0,    ! Kain-Fritsch (D01,D02 only) [20]
 cudt                          = 0,  0,  0,  0,
 isfflx                        = 1,
 ifsnow                        = 1,
 icloud                        = 1,
 surface_input_source          = 1,
 num_soil_layers               = 4,
 sf_urban_physics              = 1,  1,  1,  1,    ! SLUCM             [17]
 num_urban_layers              = 1,
/
```

A.4 Dynamics, &bdy_control, &namelist_quilt

```
&dynamics
 w_damping                     = 0,
 diff_opt                      = 1,  1,  1,  1,
 km_opt                        = 4,  4,  4,  4,
 diff_6th_opt                  = 0,  0,  0,  0,
 diff_6th_factor               = 0.12, 0.12, 0.12, 0.12,
 base_temp                     = 290.,
 damp_opt                      = 3,
 zdamp                         = 5000., 5000., 5000., 5000.,
 dampcoef                      = 0.2,   0.2,   0.2,   0.2,
 khdif                         = 0,     0,     0,     0,
 kvdif                         = 0,     0,     0,     0,
 non_hydrostatic               = .true., .true., .true., .true.,
 moist_adv_opt                 = 1,     1,     1,     1,
 scalar_adv_opt                = 1,     1,     1,     1,
/
&bdy_control
 spec_bdy_width                = 5,
 spec_zone                     = 1,
 relax_zone                    = 4,
 specified                     = .true., .false., .false., .false.,
 nested                        = .false., .true., .true., .true.,
/

&namelist_quilt
 nio_tasks_per_group           = 0,
 nio_groups                    = 1,
/
```

The setup above matches the WRF v4.6.0 build in Section 3.2 of the main text. Inline numerical references (e.g. WSM6 [25]) refer to the main reference list. WPS automatically loads the MODIFIED_IGBP_MODIS_NOAH land-use classification (61 categories) during metgrid and inherits it into namelist.input via input_from_file.

A.5 namelist.wps (WRF Preprocessing System)

The Lambert Conformal map projection, four nested domains, and ERA5 boundary-condition cadence were configured in the WRF Preprocessing System (WPS) before WRF integration. The namelist.wps file follows.

```
&share
 wrf_core         = 'ARW',
 max_dom          = 4,
 start_date       = '2025-06-21_12:00:00','2025-06-21_12:00:00',
                    '2025-06-21_12:00:00','2025-06-21_12:00:00',
 end_date         = '2025-06-23_00:00:00','2025-06-23_00:00:00',
                    '2025-06-23_00:00:00','2025-06-23_00:00:00',
 interval_seconds = 21600,
 io_form_geogrid  = 2,
/

&geogrid
 parent_id         =   1,   1,   2,   3,
 parent_grid_ratio =   1,   3,   3,   3,
 i_parent_start    =   1,  31,  45,  75,
 j_parent_start    =   1,  23,  39,  53,
 e_we              = 121, 181, 280, 385,
 e_sn              =  91, 136, 220, 310,
 geog_data_res     = 'default','default','default','default',
 dx                = 27000,
 dy                = 27000,
 map_proj          = 'lambert',
 ref_lat           =  47.918587,         ! Ulaanbaatar synoptic station
 ref_lon           = 106.848062,
 truelat1          =  30.0,
 truelat2          =  60.0,
 stand_lon         = 106.848062,
 geog_data_path    = '/home/cpl/WRF_build/WPS/WPS_GEOG',
/
&ungrib
 out_format        = 'WPS',
 prefix            = 'SURF',
/
&metgrid
 fg_name           = 'PRES','SURF',
 io_form_metgrid   = 2,
/
```

For a mid-latitude continental Asian domain, the Lambert Conformal projection centers on Ulaanbaatar synoptic station (47.92 °N, 106.85 °E) with standard parallels at 30 and 60 °N. ERA5 reanalysis fields are ingested in two streams via the ungrib step: pressure-level ('PRES') and single-level (surface) data at 6-hour cadence (interval_seconds = 21600). The metgrid step horizontally interpolates them onto the four WRF domains and writes met_em.* files to initialize WRF integration in Sections A.1–A.4.

Appendix B - URBPARM.TBL modifications

All four FRC_URB sensitivity simulations use the same namelist.input (Appendix A) and differ only in URBPARM changes.Urban canopy TBL parameter file. The WRF default MODIFIED_IGBP_MODIS_NOAH land-use mask applied to the D04 domain showed that all urban grid cells in Ulaanbaatar are HDR. All FRC_URB adjustments were made to URBPARM's HDR column. In Ulaanbaatar D04, the Low-Density Residential and Commercial/Industrial columns are inactive and default.

B.1 Other URBPARM.TBL parameters (held constant across scenarios)

The remaining urban canopy parameters were held at their WRF default values for the High-Density Residential class throughout all four simulations. The most important parameters are listed in Table B.2.

Parameter	Symbol	Value	Description
Mean building height	ZR	7.5 m	Roof height of urban canyon
Building width	BW	8.4 m	Mean horizontal width of buildings
Road width	SW	8.0 m	Mean width of street between buildings
Anthropogenic heat flux	AH	90 W/m²	Daily-mean anthropogenic heat (default)
Roof albedo	ALBR	0.20	Shortwave reflectivity of roof
Wall albedo	ALBW	0.20	Shortwave reflectivity of wall
Road albedo	ALBG	0.20	Shortwave reflectivity of road
Roof emissivity	EPSR	0.90	Longwave emissivity of roof
Wall emissivity	EPSW	0.90	Longwave emissivity of wall
Road emissivity	EPSG	0.95	Longwave emissivity of road
Roof heat capacity	CAPR	1.00E6 J/m³K	Volumetric heat capacity
Wall heat capacity	CAPW	1.00E6 J/m³K	Volumetric heat capacity
Road heat capacity	CAPG	1.40E6 J/m³K	Volumetric heat capacity
Roof thermal conductivity	AKSR	0.67 W/mK	Heat conduction
Wall thermal conductivity	AKSW	0.67 W/mK	Heat conduction
Road thermal conductivity	AKSG	0.40 W/mK	Heat conduction

Holding all parameters except FRC_URB constant ensures that differences in the simulated surface energy balance, near-surface temperature, and boundary-layer state across the four scenarios are limited to impervious fraction changes in each grid cell, not building geometry, anthropogenic heat, or urban canopy thermophysical properties.

Appendix C - Software environment

Component	Version	Purpose
Python	3.11	Programming environment
NumPy	1.26	Numerical arrays
Pandas	2.1	Time-series and tabular data
xarray	2023.12	NetCDF reading, multidimensional arrays
netCDF4	1.6	WRF wrfout file I/O
matplotlib	3.8	Figure generation
MetPy	1.6	Skew-T diagrams, atmospheric calculations
GeoPandas	0.14	Shapefile handling for maps
Cartopy	0.22	Map projections
SciPy	1.11	Interpolation and statistics